The Effect of Chemical Additives on Photovoltaic Performance of P3HT:PCBM Bulk Heterojunction Solar Cells

Eyob Daniel Shiferaw

A Thesis Submitted to the Materials Science Program

Presented in Partial Fulfillment of the Requirements for the Degree of Masters of Science in Materials Science

Addis Ababa University

Addis Ababa, Ethiopia

June 2012

Addis Ababa University

School of Graduate Studies

This is to certify that the thesis prepared by Eyob Daniel, entitled: *The Effect of Chemical Additives on Photovoltaic Performance of P3HT:PCBM Bulk Heterojunction Solar Cells* and submitted in partial fulfillment of the requirements for the degree of Degree of Masters of Science in Materials Science complies with the regulations of the University and meets the accepted standards with respect to originality and quality.

Signed by the Examining Committee:

Examiner: Gebremedhn G/Yesus (Dr) Signature _____ Date 25/06/2012

Examiner: Javed Mazher (Prof) Signature _____ Date 25.06.2012

Advisor: Teketel Yohannes (Prof) Signature _____ Date 25/06/2012

_____

Chair of Department or Graduate Program Coordinator

ABSTRACT

The Effect of Chemical Additives on Photovoltaic Performance of P3HT:PCBM Bulk Heterojunction Solar Cells

Eyob Daniel Shiferaw

Addis Ababa University, 2012

Organic bulk heterojunction solar cell devices based on blend of poly(3-hexylthiophene) (P3HT) and [6, 6] phenyl C_{61} butyric acid methyl ester (PCBM) with different concentration of propylthiouracil (PTU) additive have been fabricated and characterized in an open air. The current density-voltage characteristics were measured in the dark and under white light illumination at illumination intensity of 80 mW/cm^2. The incident monochromatic photon to current conversion efficiency (IPCE), and consistency of optical absorption and IPCE of the device without additive and with propylthiouracil have been compared. Optimizations were made by varying the concentration of propylthiouracil from 0.75% (w/w) to 1.5% (w/w). It was found that a system with 1% (w/w) of propylthiouracil showed the best photovoltaic performance with a short circuit current density, J_{SC} of 5.69 mA/cm^2, open circuit voltage, V_{OC} of 0.648 V, fill factor, FF of 40%, and power conversion efficiency (PCE), of 1.8%, as compared to the system without propylthiouracil and with other concentrations of propylthiouracil. The best device showed IPCE of 62% at 480 nm. It was also observed clearly that IPCE spectra of each solar cell match the corresponding optical absorption. Our results in general show that addition of 1% (w/w) Propylthiouracil additive to P3HT:PCBM bulk heterojunction solar cell improves efficiency of the device from 1% to 1.8%.

Acknowledgements

I would like to show my deepest gratitude to my advisor, Prof. Teketel Yohannes, who has given me the opportunity to study with an interesting subject in the field of organic solar cells.

I am very grateful to Ph.D students Getachew Adam, Sisay Tadesse, and Siraye Esubalew for their excellent guidance, sharing of expert knowledge, and experiences. Especially Getachew Adam provided me with valuable helps in every stage of this thesis.

I would like to express my sincere thanks to my friend Desalegn Jarra who gave me fruitful suggestion during the whole work. I am indebted to my colleague Bekele Haylegnaw, a graduate student in the Department of Chemistry, for his help during the laboratory work. I would like to express my sincere thanks to my family for their encouragement.

I am grateful to Wollo University for sponsoring me to join the school of graduate studies and continuous support during my study. I greatly appreciate the Department of Materials Science, Chemistry, and Physics (polymer physics larboratory), Addis Ababa University, and staff members for their sincere cooperation during my study.

Finally, I would like to express my sincere gratitude to the support and encouragement I got from my beloved Wubnesh Leta.

Table of Contents

List of Figures vii

List of Tables x

1. Introduction 1

2. Literature Review 4

2.1 Electronically Conducting Polymers 4

2.1.1 The Concept of Doping 5

2.1.2 The Origin of Semiconducting Behavior 6

2.2 Structural Distortions in Conducting Polymers 11

2.2.1 Soliton Formation 11

2.2.2 Polaron Formation 12

2.2.3 Bipolaron Formation 12

2.2.4 Charge Transport in Conjugated Polymers 14

2.3 Organic polymer Solar Cell Devices and Working Principles 16

2.3.1 Single Layer Organic Solar Cell Devices 17

2.3.2 Bilayer Organic Solar Cell Devices 19

2.3.3 Bulk Heterojunction Devices 22

2.4 Characterization of a Solar Cell Device 24

2.4.1 Current-Voltage 24

2.4.2 Spectral Response 29

2.5 Effect of additive on photovoltaic performance of BHJ solar cells 30

2.5.1 Morphology Control 30

2.5.2 Processing Additive 30

3. Objectives 33

3.1 General Objectives 33

3.2 Specific Objectives 33

4. Materials and methods 34

4.1. Materials 34

4.2. Experimental methods 35

4.3 Fabrication of solar cells 35

4.3.1 Cleaning of substrate 35

4.3.2 Preparation of solution 35

4.3.3 Spin coating 36

4.3.4. Device characterization 37

5. Results and Discussion 38

5.1 Absorption Spectra Measurement 38

5.2 Current Density-Voltage (J-V) Characteristics 40

5.3 Spectral Response 46

5.4 Comparison between Optical Absorption and Spectral Response 47

6. Conclusion 49

References 50

List of Figures

Figure 2.1: Chemical structure of some common conjugated polymers. 4

Figure 2.2: The hybridization of the valence shell electrons of a carbon atom: (a) sp^3 (b) sp^2. 8

Figure 2.3: The molecular structure of polyacetylene (top). Schematic representation of the electronic bonds in polyacetylene is depicted in the bottom panel. 9

Figure 2.4: Energy level splitting of orbitals in a conjugated polymer (a) and Collection of molecular orbitals form bands separated by an energy gap as shown in (b). 10

Figure 2.5: Left: Chemical structure of, (a) trans-polyacetylene, (b) neutral soliton, (c) positive soliton, and (d) negative soliton. Right: The corresponding band structure. . 11

Figure 2.6: Actual structures of polarons and bipolarons in polyheterocyclic polymers (X = S, O, NH, etc). 12

Figure 2.7: Energy band diagrams showing polaron and bipolaron states in the non degenerate polymer 13

Figure 2.8: Intersoliton hopping in trans-polyacetylene. 15

Figure 2.9: Single layer solar cell device 17

Figure 2.10: Band diagram of single layer solar cell device a) MIM picture b) Schottky. 18

Figure 2.11: Schematic diagram Bilayer solar cell device 19

Figure 2.12: (a) Band diagram of organic material and (b) band diagram of bilayer device 21

Figure 2.13: Dispersed heterojunction between a transparent ITO electrode and an Al electrode 22

Figure 2.14: Schematic diagram of bulk heterojunction device 23

Figure 2.15: Current-voltage (I-V) curves of an organic solar cell dark, (a) illuminated, (b) . (c) Circuit of photovoltaic device, R_S: series resistance, R_{Sh}: shunt resistance.....24

Figure 2.16: Semi logarithmic current density-voltage characteristics of non illuminated bulk heterojunction device.....28

Figure 4.1: Chemical structure of substances used in this work.....34

Figure 4.2: Basic device structure of bulk heterojunction solar cell used in this study. 36

Figure 5.1: Normalized absorbance of thin films of P3HT:PCBM with different concentration of propylthiouracil.....39

Figure 5.2: Semilogarithmic current density-voltage characteristics of bulk heterojunction device of structure ITO/PEDOT:PSS/P3HT:PCBM with different concentration of propylthiouracil/Al. 40

Figure 5.3: The J-V characteristics of ITO/PEDOT:PSS/P3HT:PCBM/Al, based BHJ solar cell with different concentration of propylthiouracil additive in the dark and under white light illumination with incident light intensity of 80 mW/cm^2.....41

Figure 5.4: Semilogarithmic J-V characteristics of ITO/PEDOT:PSS/P3HT:PCBM /Al, based BHJ solar cell with different concentration of propylthiouracil additive in the dark and under white light illumination with incident light intensity of 80 mw/cm^2. 42

Figure 5.5: Current density-voltage characteristics of bulk heterojunction device of structure ITO/PEDOT:PSS/P3HT:PCBM/Al, in the dark and under white light illumination with incident light intensity of 80 mw/cm^2. 44

Figure 5.6: Semilogarithmic current density-voltage Characteristics of bulk heterojunction device of structure ITO/PEDOT:PSS/P3HT:PCBM/Al, in the dark and under white light illumination with incident light intensity of 80 mW/cm^2.....45

Figure 5.7: IPCE spectra of bulk heterojunction device of structure ITO/PEDOT: PSS/P3HT:PCBM/Al, with different concentration of propylthiouracil additives.....46

Figure 5.8: IPCE spectra of bulk heterojunction device of structure ITO/PEDOT: PSS/P3HT: PCBM/Al. (a) without additive (b) with 0.75% (w/w) propylthiouracil (c) with 1% (w/w) propylthiouracil (d) with 1.5% (w/w) propylthiouracil (e) absorption spectra of P3HT:PCBM. 47

List of Tables

Table 1: The typical photovoltaic performance parameters of P3HT:PCBM with different concentration of propylthiouracil additive at illumination intensity of 80 mw/cm^2. 42

1. Introduction

The energy demand of our globe is increasing rapidly with increasing human population, urbanization, and modernization. At present, the world energy consumption is 10 terawatts (TW)/yr, and by 2050, it is projected to be about 30 TW/yr [1]. Currently, close to 80% of the energy supply worldwide is based on fossil fuels like coal, oil and gas which are not renewable sources [2]. The transformation of these resources into usable energy induces massive CO_2 emissions, which is the main cause of the greenhouse effect. Moreover, the price of oil and gas is increasing dramatically; while reserves of fossil fuel are declining [3]. Renewable energies are one of the most important components of the global new energy strategy. Solar energy, the so-called truly green energy, with almost unlimited supply capability, is widely distributed all over the earth. Having these prominent advantages, the worldwide researches on the solar energy have become one of the hottest scientific topics.

The annual amount of energy that the earth receives from the sun is enormous i.e. , $3.9\times\ 10^{24}$ J. The earth receives enough energy to fulfill the yearly world demand of energy in less than an hour [4]. Many techniques have been developed to harness the power of the sun. Photovoltaic is a technology which actively transforms the sun's energy directly into electricity using solar cells [5]. Historically, conventional solar cells were built from inorganic materials such as silicon. The efficiency of such conventional solar cells made from inorganic materials reached upto 25% [6]. But the production costs are too high for widespread energy production using these devices. Thin film technique should reduce material consumption. Typical materials which are used in thin film photovoltaic, devices are inorganic semiconductors like silicon,

cadmium telluride and copper indium diselenide [7]. Generally all these inorganic semiconductors need high temperature operations in their production, which causes high cost, and are difficult to handle. Therefore, to insure a sustainable technology for solar cells, the development of new materials and device structures are required. A promising approach towards low production cost of photovoltaic device is fabrication of solar cells based on organic materials [8]. The interest in organic solar cells has risen strongly in recent years due to their interesting properties in terms of low cost synthesis, flexibility, easy manufacture of solution cast technologies [9] and high absorption coefficients exceeding 10^5 cm^{-1} [10].

The large exciton binding energy in a polymeric matrix results in strongly bounded electron hole pairs upon light absorption, giving rise to the small exciton diffusion length and inefficient exciton dissociation [11]. Therefore, a major challenge lies in fabricating polymer solar cells, in which free charge carrier generation is a critical step. Fortunately, it has been found that efficient charge transfer can take place between materials, that is, donor and acceptor molecules, with suitable energy level offsets. The strong electric field at the molecular interface of two materials with different electrochemical potentials is capable of separating the excitons into weakly bounded Coulombic pairs, and thereafter separated charge carriers. In cases where the donor and acceptor molecules form an intimate contact in blend films, efficient charge transfer takes place [12].

The bulk heterojunction concept is employed to overcome the short exciton diffusion distance. The photoactive film of heterojunction is formed from the donor and acceptor materials which are phase separated on the nanometer length scale, to

facilitate the photo induced charge transfer as well as create a percolating pathway for charge transport to the electrodes [13]. Therefore, the nanomorphology of polymer solar cells plays a crucial role for the performance of the devices.

Historically, thermal annealing of the film has been used to induce the phase separation between donor and acceptor in bulk heterojunction blends [14]. However, thermal treatment creates an additional fabrication step in the whole device fabrication process. Later, various methods have been tested and employed to control the nanomorphology of the blends, namely use of solvents with different boiling points (choice of solvent), reduction of drying speed (rate of drying and vapor annealing), changing the solubility of materials, and the use of processing additives [15]. The later method has received great academic interest as it removes the need for postproduction treatment while at the same time allowing fine control of the nanomorphology in various donor acceptor blends [16].

In this work the effect of chemical additive (propylthiouracil) on photovoltaic characteristics of bulk heterojunction solar cells based on poly(3-hexylthiophene) (P3HT) and [6, 6]-phenyl C_{61} butyric acid methyl ester (PCBM) is studied.

2. Literature Review

2.1 Electronically Conducting Polymers

Polymers, by virtue of their light weight and greater ease of fabrication, have replaced and are continuing to replace metals in several areas of applications; as often remarked 'from buckets to rockets'. Polymers have traditionally been considered good electrical insulators and a variety of their applications have relied on this insulating property. However, there are some polymers which become electrically conducting, if they are treated with strong oxidizing or reducing agents. The chemical structures of some common polymers are shown in Figure 2.1. A common feature of all of them is the existence of conjugated double bonds (those that possess an extended π-conjugation along the polymer backbone). Typical oxidizing agents are I_2, Br_2, AsF_5, SbF_5 and $FeC1_3$ and the typical reducing agents are the alkali metals. Usually the trans form of polyacetylene is considered as the prototype of conducting polymers [17].

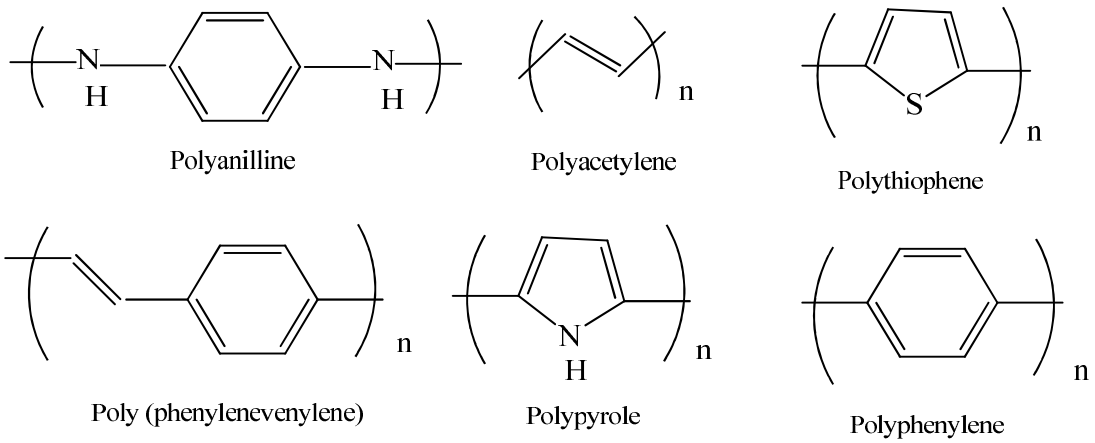

Figure 2.1: Chemical structure of some common conjugated polymers.

2.1.1 The Concept of Doping

Conjugated organic polymers are either electrical insulators or semiconductors. Those that can have their conductivity increased by several orders of magnitude from the semiconductor regime are generally referred to as "electronic polymers" [18]. The concept of doping is the unique, central, underlying, and unifying theme which distinguishes conducting polymers from all other types of polymers [19]. During the doping process, an organic polymer, either an insulator or semiconductor having a small conductivity, typically in the range of 10^{-10} to 10^{-5} Scm^{-1}, is converted into a polymer which is in the "metallic" conducting regime (ca. 1 to 10^{4} Scm^{-1}). The controlled addition of known, usually small ($\leq$10%) non stoichiometric quantities of chemical species results in dramatic changes in the electronic, magnetic, optical and structural properties of the polymer.

By controllably adjusting the doping level, a conductivity anywhere between that of the non-doped (insulating or semiconducting) and that of the fully doped (highly conducting) form of the polymer can be easily obtained. This permits the optimization of the best properties of each type of polymer. Doping can be accomplished in a number of ways [20].

A. Chemical doping by charge transfer
B. Electrochemical doping
C. Doping of polyaniline by acid-base chemistry
D. Photodoping
E. Charge injection at a metal-semiconducting polymer (MS) Interface

Doping introduces carriers into the electronic structure. Since every repeat unit is a potential redox site, conjugated polymers can be doped n-type (reduced) or p-type (oxidized). The basic processes in chemical doping for example are shown in a and b.

p-type

$$(\pi - polymer)_n + \frac{3}{2}ny(I_2) \rightarrow \left[(\pi - polymer)^{+y}\left(I_3^{-}\right)_y\right]_n \quad \text{(a)}$$

n-type

$$(\pi - polymer)_n + \left[Na^{+}(Napthtalide)\right]_y \rightarrow \left[\left(Na^{+}\right)_y(\pi - polymer)^{-y}\right]_n + (Naphth)^0 \quad \text{(b)}$$

When doping level is sufficiently high, the electronic structure evolves to that of a metal.

2.1.2 The Origin of Semiconducting Behavior

Since carbon atom (C-atom) is the main building block of most organic polymers, the type of bonds that its valence electrons make with other C-atoms or other elements determines the overall electronic properties of the respective polymer. Polymers can, in general, be categorized as saturated and unsaturated based on the number and type of the carbon valence electrons involved in the chemical bonding between consecutive C-atoms along the main chain of the polymers. Saturated polymers are insulators since all the four valence electrons of C-atom are used up in covalent bonds, whereas most conductive polymers have unsaturated conjugated structure. π-conjugated polymers are excellent examples of unsaturated polymers whose electronic configuration stems from their alternate single and double carbon-carbon bonds.

The fundamental source of semiconducting property of conjugated polymers originates from the overlap of the molecular orbitals formed by the valence electrons of chemically bonded C-atoms. A neutral carbon atom has six electrons, which occupy the 1s, 2s and 2p orbitals giving a ground state electronic configuration of $1s^2 2s^2 2p^2$ [1s (↑↓) 2s (↑↓) 2p (↑) (↑)]. The atomic orbitals of carbon are modified into hybrid orbitals as they form covalent bonds (Figure 2.2). When a carbon atom forms a bond with another carbon atom, a 2s-electron is promoted to the vacant 2p orbital resulting into a $2s^1 2p_x^1 2p_y^1 2p_z^1$ configuration as depicted in Figure 2.2. These electronic orbitals do not bond separately but hybridize, i.e. mix in linear combinations, to produce a set of orbitals oriented towards the corners of a regular tetrahedron. The hybrid orbitals consisting of one s orbital and three p orbitals are known as sp^3 hybrid orbitals.

The sp^3 hybrids allow a strong degree of overlap in bond formation with another atom and this produces high bond strength and stability in the molecules. The arrangement of bonds resulting from overlap with sp^3 hybrid orbitals on adjacent atoms gives rise to the tetrahedral structure that is found in the lattice of diamond and in molecules such as ethane, C_2H_6. In these structures all the available electrons are tied up in strong covalent bonds, named σ-bonds. Carbon compounds containing σ-bonds formed from sp^3 hybrid orbitals are termed saturated molecules. The saturated hydrocarbons, in general, have high band gaps and, hence, are classified as insulators [21].

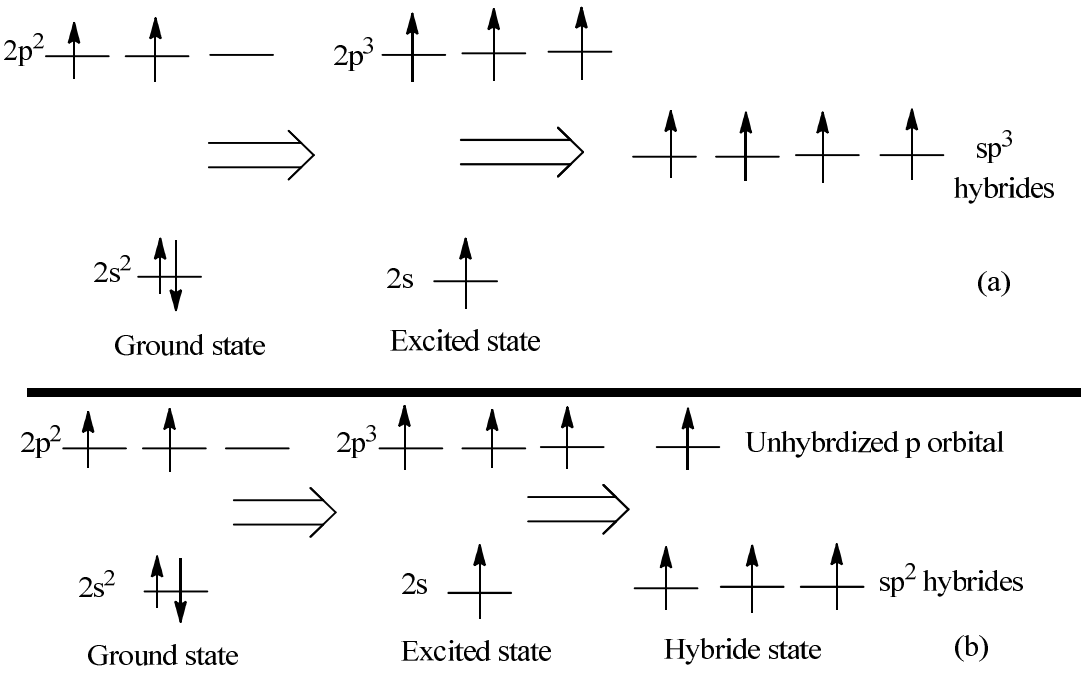

Figure 2.2: The hybridization of the valence shell electrons of a carbon atom: (a) sp^3 (b) sp^2.

Since conjugated polymers composed of alternating single and double bonds, sp^3 hybridized orbitals cannot account for their electronic structure. The alternating single and double bonds are formed from sp^2 hybrid orbitals. Mixing of one *s* orbital with two of the p orbitals of C-atom forms three sp^2 hybrid orbitals, leaving one p orbital unhybridized (Figure 2.2). The sp^2 carbon hybrid orbitals are known to form a different bond length, strength, and geometry when compared to those of the sp^3 hybridized molecular orbitals. The sp^2 hybridization has one unpaired electron (π-electron) per C-atom. The three sp^2 hybrid orbitals of a C-atom arrange themselves in three-dimensional space to attain stable configuration. The geometry that achieves this is trigonal planar geometry, where the bond angle between the sp^2 hybrid orbitals is 120^o. The unmixed pure p_z orbital lies perpendicular to the plane of the three sp^2 hybrid orbitals (Figure 2.3). The sp^2 orbitals give σ-bonds while the p_z orbitals form a

different type of bonds known as π-bonds. The p_z orbitals of a polymer exhibit π-overlap, which results into a delocalization of an electron along the polymer chain. The π-bonds are, thus, considered as the basic source of transport band in the conjugated systems [20, 21]. Polyacetylene is often considered as a model conjugated polymer. It has a simple, linear structure and exhibits a degenerate ground state. Figure 2.3 illustrates the arrangement of the σ-bonds and π-bonds in polyacetylene. Owing to its structural and electronic simplicity, polyacetylene is well suited to semi-empirical calculations and has therefore played a critical role in the elucidation of the theoretical aspects of conducting polymers [22].

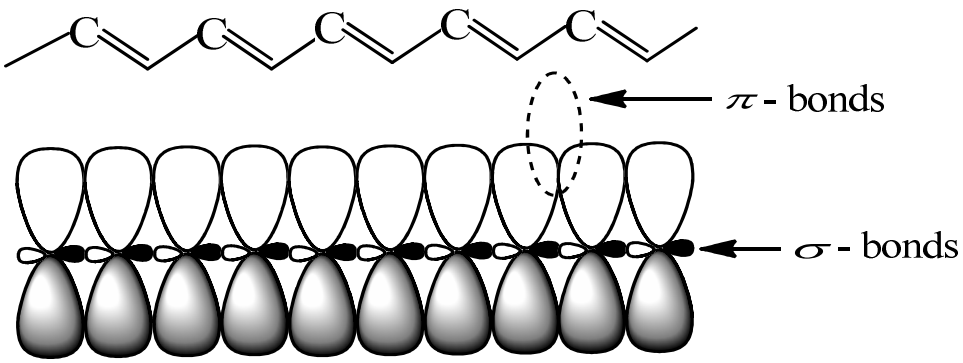

Figure 2.3: The molecular structure of polyacetylene (top). Schematic representation of the electronic bonds in polyacetylene is depicted in the bottom panel.

In terms of an energy-band description, the σ-bonds form completely filled bands, while π-bonds would correspond to a half -filled energy band (Figure 2.4). The molecular orbitals of a polymer form a continuous energy band that lies within a certain energy range. The anti-bonding orbitals located higher in energy (π*) form a conduction band whereas the lower energy lying bonding orbitals form the valance band. The two bands are separated by a material specific energy gap known as a *band gap* (E_g) (Figure 2.4). The two separate bands are characterized by two quite

important energy levels, namely electron affinity and ionization potential. The electron affinity of a semiconducting polymer corresponds to the lowest state of the conduction band (π* state) or the lowest unoccupied molecular orbital (LUMO). Likewise, the ionization potential refers to the upper state of the valence band (π state) and corresponds to the highest occupied molecular orbital (HOMO).

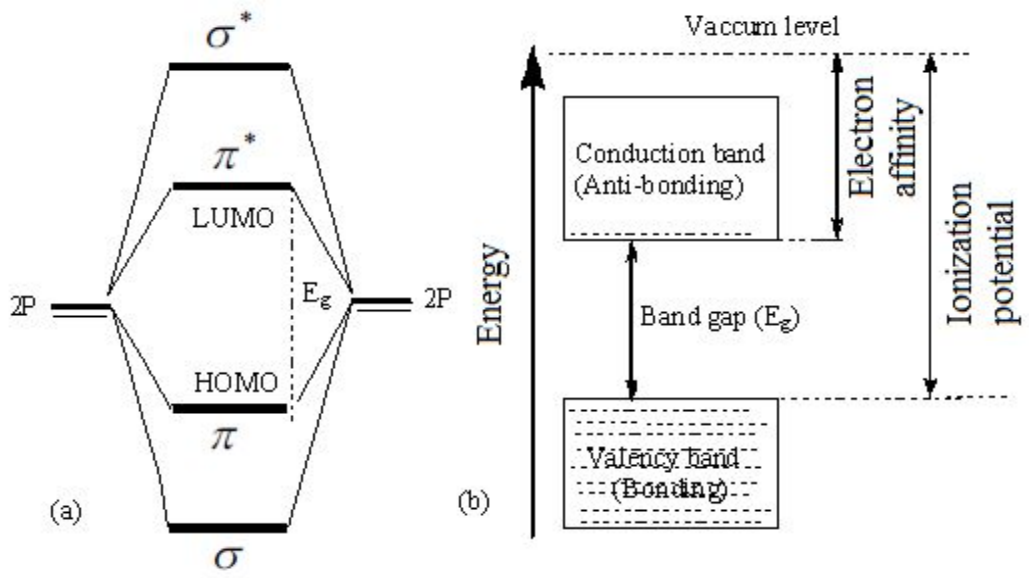

Figure 2.4: Energy level splitting of orbitals in a conjugated polymer (a) and Collection of molecular orbitals form bands separated by an energy gap as shown in (b).

The band gap of conjugated polymers determined from optical, electrochemical and other spectroscopic measurements is within the semiconductor range of 1 to 4 eV [21], which covers the whole range from infrared to ultraviolet region. Conjugated Polymers are often considered as quasi-one dimensional metals due to the fact that the strong intrachain interaction (strong covalent bonding along the chain), and the weak Van der Waals type interchain coupling interactions lead to delocalization of π-electrons along the polymer chain [20-22].

2.2 Structural Distortions in Conducting Polymers

2.2.1 Soliton Formation

When combining two chain segments of trans-polyacetylene (Figure 2.5) having different bond order (the ground states are degenerate), a defect in the form of an unpaired electron will be formed. Such a defect, having charge zero and spin 1/2, is called a soliton [23]. The unpaired electron is accompanied by bond length distortions in a region over about 15 carbon atoms [24, 25]. The distortion of the chain results in the formation of a new localized energy level in the middle of the band gap that is occupied by the unpaired electron. There are also positively charged and negatively charged solitons with zero spin [26, 27].

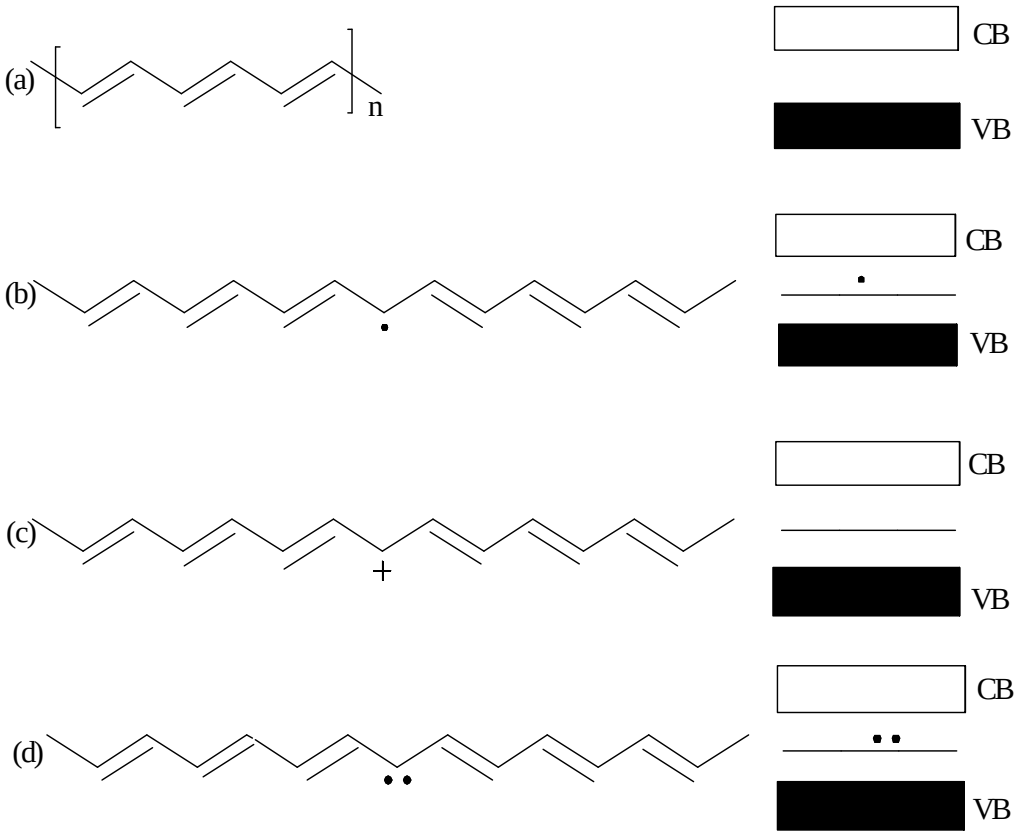

Figure 2.5: Left: Chemical structure of, (a) trans-polyacetylene, (b) neutral soliton, (c) positive soliton, and (d) negative soliton. Right: The corresponding band structure.

2.2.2 Polaron Formation

Localized distortion of a conducting polymer with non-degenerate ground states and possessing a standard semiconductor band structure gives rise to two localized electronic states in the region between the valence and the conduction bands followed by a small local upward shift of the HOMO (i.e. the valence band) and downward shift of the LUMO (i.e. the conduction band). In a conducting polymer with non-degenerate ground states, removal of an electron from this localized state (i.e. oxidation or p-doping) forms an entity called a polaron [28]. A polaron is a radical cation (one unpaired electron), which is locally associated with a structural distortion in the conducting polymer (Figure 2.6). A hole polaron, created upon p-doping of the polymer has a charge of +1 and a spin of 1/2. The lower level of the sub-gap states is half occupied and the upper level is empty (Figure 2.7).

2.2.3 Bipolaron Formation

At higher doping levels, further removal of electrons preferably forms a bipolaron (two positive charges) (Figure 2.6) rather than two polarons [29]. The stability of the bipolaron, despite the coulombic repulsion between the two positive charges, is considered to arise from electron-phonon coupling [30]. A hole bipolaron has a charge of +2 and a zero spin. Both of the sub-gap states are empty (Figure 2.7).

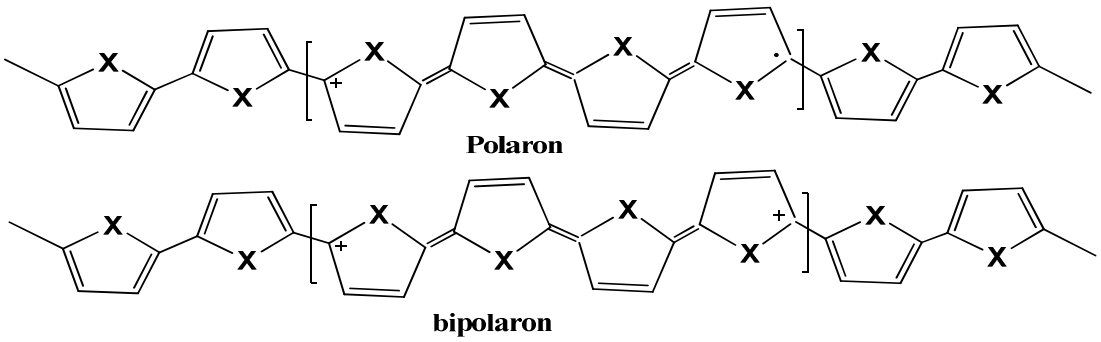

Figure 2.6: Actual structures of polarons and bipolarons in polyheterocyclic polymers (X = S, O, NH, etc).

We may also have *n*-doping, i.e. reduction or donation of electrons to the conducting polymer chain. We would then have negatively charged polarons and bipolarons. n-doping gives a doubly occupied lower level and a singly occupied upper level (for n-polaron) or a fully occupied higher level (for n-bipolaron) of the sub-gap states (Figure 2.7). Bipolarons can be mobile and can propagate along the conducting polymer chain. Thus at sufficient concentration levels, they can function as charge carriers. They are delocalized over some (6 to 8) monomer units [31]. As one progresses further to very high doping levels, the individual bipolaron states coalesce into bipolaron bands. At these high dopant concentrations, the bipolarons can become mobile under the application of an electric field, thus giving rise to the high conductivity observed in conducting polymers.

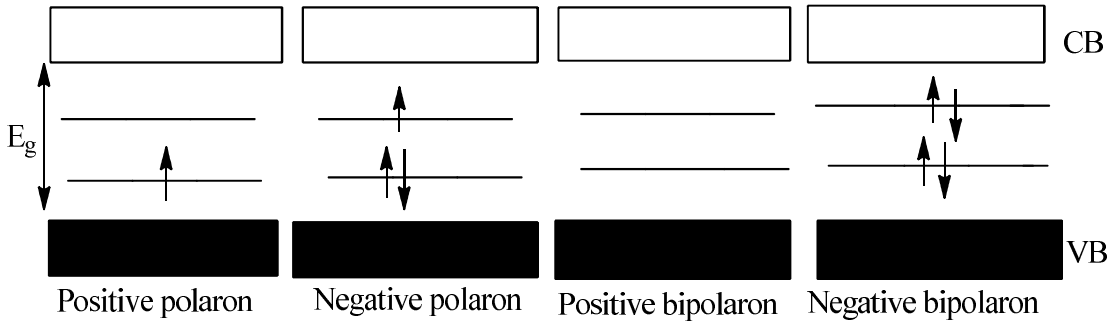

Figure 2.7: Energy band diagrams showing polaron and bipolaron states in the non degenerate polymer [32].

At maximum doping levels, the bipolaron bands of conjugated polymers with low band gaps ($\approx$2 eV), such as polythiophenes, can merge with the valence and conduction bands, producing metal like conduction stemming from the lower, half-filled valence/bipolaron band [33].

Polarons, bipolarons and other structural distortions in conducting polymers may be most commonly generated by electrochemical or chemical doping with appropriate counter ions then taking their place in the vicinity of these for charge neutrality [24]. Another method of generating these sub-gap states is through irradiation, which is called photodoping. When conducting polymers are irradiated with light of energy greater than or equal to the band gap, electrons will be excited to the conduction band leaving a hole in the valence band. The electrons and holes remain bound forming an electron–hole pair. This bound electron-hole pair in a polymer chain is called an exciton. An exciton may recombine (thermally or radiatively) or separate to give free charges.

2.2.4 Charge Transport in Conjugated Polymers

Conductivity of materials depends on temperature. For pure metals conductivity increases with decreasing temperature because of lattice vibrations, which act as obstacles for the charge carriers, freeze out when cooling the metal. On contrary, cooling of an intrinsic crystalline semiconductor decreases its electrical conductivity. This attributed to the fact that cooling freeze out not only lattice vibration but also charge carriers. In amorphous semiconductors there is no continues carriers motion at all. This carriers are localized, and can only move with the help of lattice vibrations consequently the electrical conductivity increases with increasing temperature, but it doesn't increase exponentially as crystalline semiconductors [34]. In conducting polymers the conductivity is due to the presence of solitons, polarons and bipolarons, which are formed by self localization of carriers introduced in to π-electronic systems through doping [22]. The temperature dependence of the conductivity of conducting polymers appears to be quite different at different doping levels [35]. Lightly doped or

un-doped conducting polymers show strong temperature dependence of the conductivity. The room temperature conductivity is low and its conductivity vanishes at 0 K.

There is no definite mechanism of charge transport and hence different models are suggested over the whole conductivity range. In the undoped form of conjugated polymers, the charge transport is similar to that of amorphous semiconductors. It is explained by hopping between localized states. At very low doping levels, the conductivity is mainly due to hopping. Its concept is generally deduced from ionic conduction to electronic conduction in amorphous and disordered non-metallic solids and polymers. In such materials we do not have free charge carriers, rather than localized electrons and so they can move between these localized states which are distributed randomly.

For polyacetylene, where solitons are dominant charge carriers, intersoliton hopping is the dominant conductivity mechanism. The solitons may be either neutral or charged, see Figure 2.8.

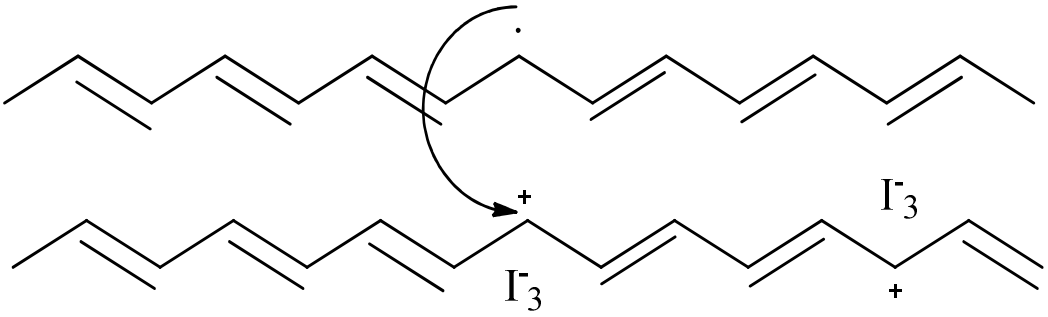

Figure 2.8: Intersoliton hopping in trans-polyacetylene.

The charged solitons are trapped by the dopant ions and neutral solitons are free to move. When neutral soliton passes close by a charged soliton, an electron can hop between the mid gap states belonging to the solitons [36].

2.3 Organic polymer Solar Cell Devices and Working Principles

The conversion process of light energy to electric current in organic solar cells is accomplished by four sequential steps [37].

1. Absorption of light photon leads to the formation of excited state, the electron-hole pair called excitons.
2. Diffusion of exciton to the region where dissociation may occur.
3. Dissociation of electron-hole pair (excitons) to form free charges.
4. Charge (electrons and holes) transport.

Light absorption in conjugated polymer excites electrons to a state above band gap. This results in the formation of excitons. In this state, electrons and holes are tightly bonded by columbic attraction forces. The binding energy of excitons is ≈ 0.4 eV [38]. These excitons can diffuse through the polymer in the range of 10 nm before vanishing. These excitons must be dissociated in order to obtain free charge carriers before they vanish. To break up the excitons, an electric field of energy greater than the binding energy of the electron-hole pair is required. Dissociation of excitons at a heterojunction interface can generate free charge carriers. Combinations of acceptor and donor conjugated materials, conjugated material/metal layer and conjugated material/inorganic particles blend act as good interfaces for efficient dissociation of excitons due to the formation of an electric field at the junction [37]. In the following, the most basic device architectures are reviewed, and the individual advantages and

disadvantages are discussed. Their main difference lies in the exciton dissociation or charge separation process, which occurs at different locations within the photoactive layer. A second issue is the consecutive charge transport to the electrodes.

2.3.1 Single Layer Organic Solar Cell Devices

Single layer organic solar cells are the simplest form of organic solar cells. These solar cells are fabricated by sandwiching a layer of conjugated material between two metallic conductors. The basic structure of the device is shown in Figure 2.9. The device consists of a polymer active layer sandwiched between a high work function indium doped tin oxide (ITO) electrode and a low work function Al or Mg or Ca electrode. In 1994, this structure was created by R. N. Marks *et al*. using 50-320 nm thickness of poly (p-phenylene vinylene) (PPV) sandwiched between an ITO and a low work function cathode [39].

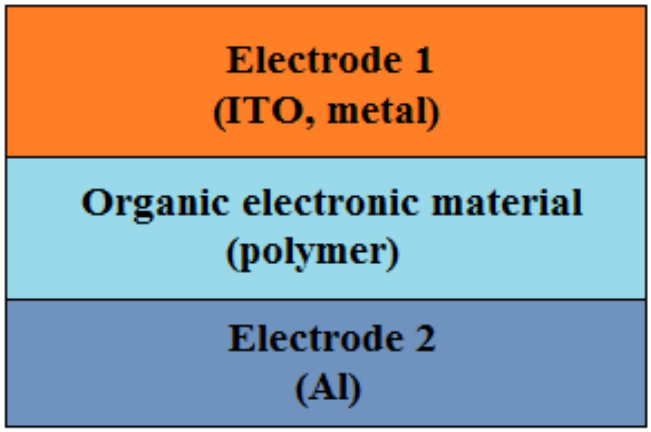

Figure 2.9: Single layer solar cell device [23].

The selection of the electrodes determines the characteristics of the solar cell. Work function of the devices is the key parameter in analyzing the device behavior. The

difference in the work functions of electrodes creates the electric field to dissociate the excitons. Work function is the energy difference between the vacuum level and Fermi level of the material. The rectifying behavior of the device is explained by using a MIM (metal insulator metal for insulators) picture or schottky barrier (for doped materials) as shown in Figure 2.10.

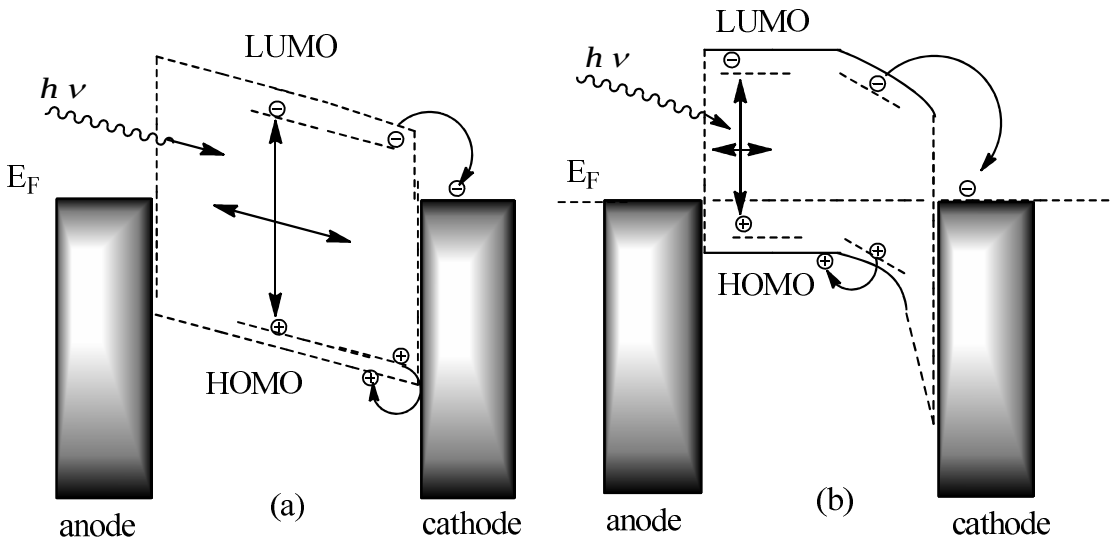

Figure 2.10: Band diagram of single layer solar cell device a) MIM picture b) Schottky.

When polymer absorbs the light photons, electrons are excited to LUMO level and leave holes in HOMO level. The work function difference between the electrodes sets up an electric field. Band bending occurs at the junction of the Schottky barrier formed between the low work function metal and the polymer layer due to the electric field generated by the work function difference. The excitons are dissociated in the depletion region of the Schottky barrier.

The problem with a single layer organic solar cells device is that it demonstrates low efficiencies. These types of cells have quantum efficiencies less than 1% and power conversion efficiencies of less than 0.1%. These low efficiencies are due to the inefficient dissociation of excitons. The electric field generated between the electrodes is not sufficient to dissociate the excitons. Frequently, generated holes recombine with the electrons before reaching the electrodes. Bilayer devices were designed to address this problem.

2.3.2 Bilayer Organic Solar Cell Devices

A bilayer solar cell includes two different organic layers sandwiched between the two conductive electrodes. In 1986, C.W. Tang first reported on the bilayer heterojunction organic solar cells based on the Cu-phthalocyanine (CuPc)/perylene tetracarboxylic derivative (PV) [40]. In 1992, Sacriciftci et al. found that C_{60} can be a good electron acceptor material [9]. Soon after, these organic solar cells, which uses C_{60} and its derivatives as an electron acceptor became widespread [41 - 43]. Figure 2.11 shows the basic structure of the device.

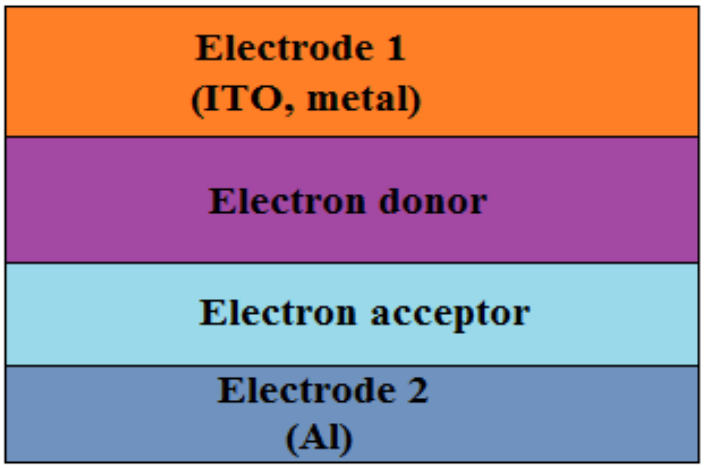

Figure 2.11: Schematic diagram Bilayer solar cell device [23].

These solar cells are also called as planar-donor-acceptor heterojunction solar cells. The donor and acceptor planar interface acts the location for the exciton dissociation. These materials are chosen so that the materials have different ionization potentials and electron affinities. These differences create electrostatic forces at the interface. Donor and acceptor materials are chosen to make the differences large enough, so these electric fields are strong, which may break up the excitons more efficiently than the single layer devices do. Acceptors have higher electron affinity and ionization potentials than the donor material does. Upon absorption of incoming light by the donor layer, electrons in the donor material are excited from HOMO level to LUMO level and form excitons. If an acceptor molecule is in proximity of the excitons it can be transferred to the LUMO of the acceptor and can be dissociated at the interface. This transfer can occur when the ionization potential (I_{D^*}) of excited state of donor satisfies the following non linear equation.

$$I_{D^*} - A_A - U_C < 0 \tag{1}$$

Where

I_{D^*} is the ionization potential of the excited state of the donor.

A_A = Electron affinity of acceptor material.

U_C = Effective columbic interaction.

The energy diagram shown in Figure 2.12 depicts the maximum voltage that can be obtained from the device. Absorption of photons leads to the excitation to a high energy level whereas the charge separation at the planar interface lowers the energy of the charge carriers gained from the absorption. As shown in Figure 2.12 the maximum energy obtained is the difference between the LUMO level of the acceptor material

and the HOMO level of the donor material. This energy difference is often called the effective band gap $E_{g,\ eff}$ of the planar junction.

Mono molecular transport is the biggest advantage of bilayer devices over single layer devices. After the excitons are dissociated at the heterojunction interface, electrons pass through n-type material and holes pass through p-type material to the external circuit. Electrons and holes are effectively separated from each other, and hence, carrier recombination is greatly reduced. This recombination only depends on the trap densities. Traps are the vacancies which absorbs the electrons and holes.

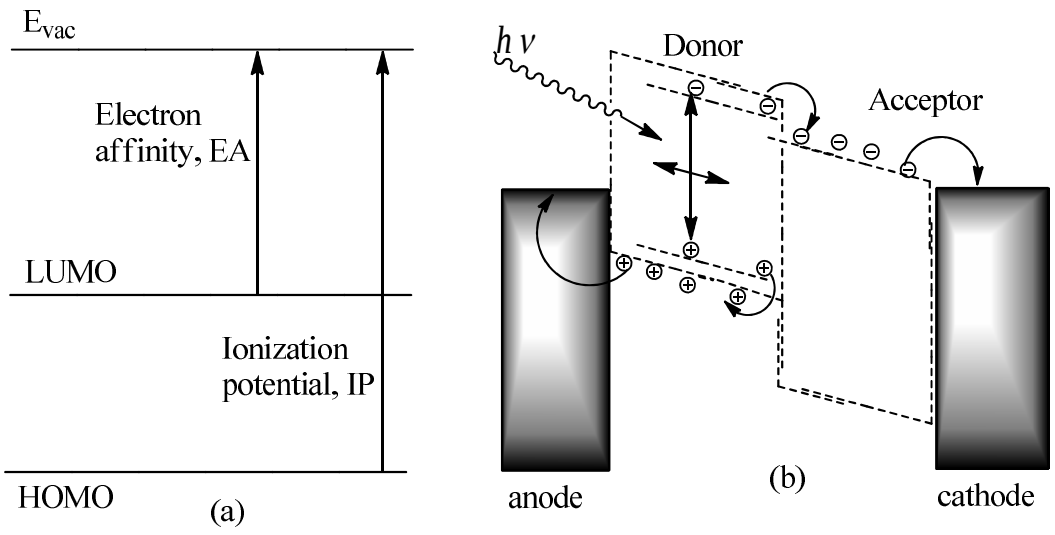

Figure 2.12: (a) Band diagram of organic material and (b) band diagram of bilayer device [38].

The main problem of these heterojunction devices is the short diffusion length of exciton in these materials. The diffusion length of excitons in polymers is in the order of 10 nm. For effective dissociation of excitons, the thickness of the layers must be in the same range as this diffusion length. However, the organic material layer needs a

minimum thickness of 100 nm to absorb enough photons. At 100 nm thickness, only a small percentage of excitons reach the interface junction. Bulk heterojunction devices were designed to address this problem.

2.3.3 Bulk Heterojunction Devices

The planar donor-acceptor junction only doubles the active region of the solar cell with respect to the single layer device, which is still usually not enough for efficient light absorption. To overcome this problem and to increase the optical thickness of the film while maintaining efficient current collection at the same time, the concept of interpenetrating network of electron accepting and electron-donating molecular species was developed and demonstrated successfully in number of different so-called donor-acceptor blend devices [44, 45].

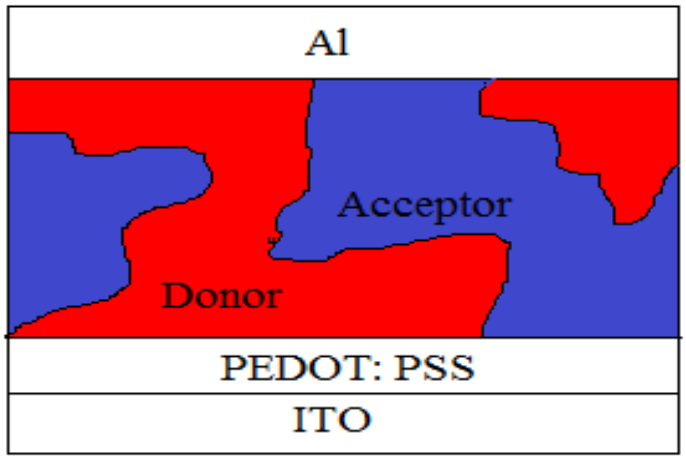

Figure 2.13: Dispersed heterojunction between a transparent ITO electrode and an Al electrode [46].

In this type of device, electron acceptor and donor materials are mixed together, and forms a polymer blend. If the length of the blend is same as that of the diffusion length of excitons, then most of the generated excitons will reach the donor and acceptor interface. This phenomenon leads to efficient dissociation of excitons. Holes

move to the donor domains then are transported through the device and collected by the anode, and electrons are transported in the opposite direction and collected at the cathode. The bulk heterojunction structure is similar to the bilayer structure with respect to donor to acceptor concept, but it has largely increased interfacial area where exciton dissociates. For transportation of charges, acceptor and donor phases have to form an interpenetrating and bicontinuous network. So the performance of the device is highly dependent upon the nanomorphology of the blend. The excitons created by absorption of photons are everywhere in the bulk. These excitons are in proximity to the interface between the materials. Therefore, efficient dissociation of excitons and charge separation can occur everywhere in the bulk of the heterojunction layer. Figure 2.14 shows the energy levels of donors (shown in dark dashed lines), the energy levels of acceptors (shown in light dashed lines), and the mechanism of photocurrent generation. Electrodes have to be chosen such that the work function of one electrode is close to the LUMO level of the acceptor and the other electrode forms good contact with the HOMO level of donor material. The maximum voltage obtained from the device is the difference of LUMO of acceptor and HOMO of donor.

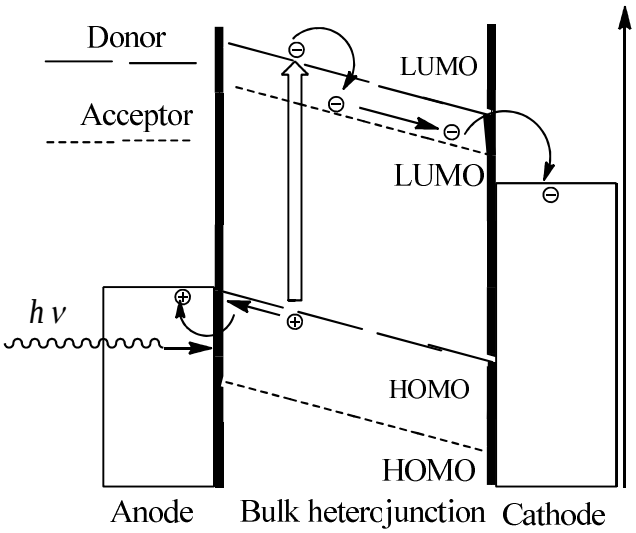

Figure 2.14: Schematic diagram of bulk heterojunction device [47].

The disadvantages are that it is somewhat more difficult to separate still strongly coulomb bound charge carrier pairs due to the increased disorder, and that percolation to the contacts is not always given in the disordered material mixtures. Also, it is more likely that trapped charge carriers recombine with mobile ones. However, the positive effects on the device performance outweigh the drawbacks and showed a power conversion efficiency of 8.3% [48].

2.4 Characterization of a Solar Cell Device

2.4.1 Current-Voltage

The typical current-voltage characteristics of a solar cell in the dark and under illumination are shown in Figure 2.15. Under dark conditions, there is no current at the short circuit condition. Under an illumination condition, the incident photons generate current and the minus current density in the fourth quadrant of J-V curve indicates this photogenerated current.

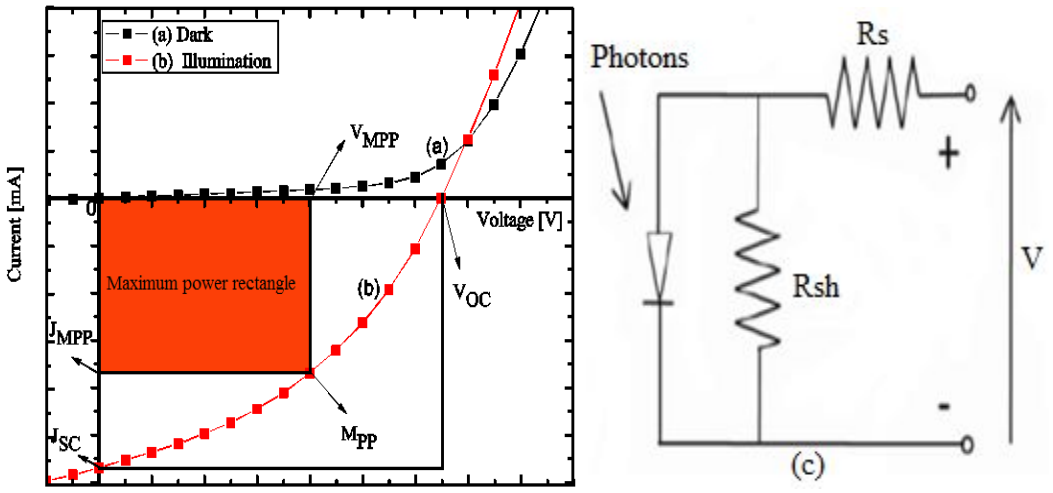

Figure 2.15: Current-voltage (I-V) curves of an organic solar cell dark, (a) illuminated, (b) [8]. (c) Circuit of photovoltaic device, R_S: series resistance, R_{Sh}: shunt resistance.

Parameters such as short circuit current density (J_{SC}), open circuit voltage (V_{OC}), fill factor (FF), and power conversion efficiency (PCE) are used to quantitatively analyze the performance of solar cells. For an ideal diode, the dark current density J_{dark} (V) is given by

$$J_{dark}(V) = J_0\left(e^{\frac{qV}{k_B T}} - 1\right) \tag{2}$$

Where J_0 is a constant, k_B is Boltzmann's constant and T is temperature in degrees Kelvin.

The overall current voltage response of the cell can be approximated as the sum of the short circuit photocurrent and the dark current. Although the reverse current, which flows in response to voltage in an illuminated cell, is not formally equal to the current that flows in the dark, the approximation is reasonable for many photovoltaic materials. The sign convention for current and voltage in photovoltaics is that the photocurrent is negative. With this sign convention, the net current density in the cell is

$$J(V) = J_{SC} - J_{dark}(V) \tag{3}$$

which becomes, for an ideal diode.

$$J(V) = J_{SC} - J_0\left(e^{\frac{qV}{k_B T}} - 1\right) \tag{4}$$

Short circuit current (J_{SC})

This is the current that flows through an illuminated solar cell when there is no external resistance (i.e., when the electrodes are simply connected or short-circuited). The short-circuit current is the maximum current that a device is able to produce.

Under an external load, the current will always be less than J_{SC}. Factors that lower short circuit current are mainly due to the spectral mismatch between the sunlight and the absorption spectrum of the polymers and fullerenes used, as well as the limited transport of the separated charge carriers to the electrodes due to the low charge carrier mobility in organic materials.

Open circuit voltage (V_{OC})

It is the maximum voltage attainable in a solar energy conversion device. The cell is placed in an open-circuit and illuminated. Electrons and holes separate and flow towards the low and high work function materials, respectively. At some point the charge build-up will reach a maximum equal to the V_{OC}. At open-circuit voltage, the net current J is zero. For the ideal diode,

$$V_{OC} = \frac{kT}{q} \ln\left(\frac{J_{SC}}{J_0} + 1\right) \tag{5}$$

Equation (5) shows that V_{OC} increases logarithmically with light intensity.

In general, V_{OC} is limited by several factors including interfacial energy levels, shunt losses, interfacial dipoles, and morphology of the active film. For donor/acceptor based solar cells with Ohmic contacts, V_{OC} is mainly determined by the difference between the HOMO of the donor polymer and the LUMO of the acceptor molecule indicating how much the electronic levels are crucial in determining the efficiency of such solar cells.

Fill factor (FF)

The ratio of a photovoltaic cell's actual maximum power output to its theoretical power output if both current and voltage were at their maxima, J_{SC} and V_{OC}, respectively. This is a key quantity used to measure cell performance. It is a measure

of the squareness of the J–V curve. The formula for FF in terms of the above quantities is:

$$FF = \frac{J_{MPP} V_{MPP}}{J_{SC} V_{OC}} \tag{6}$$

For a high FF, two things are required: (i) that the shunt (parallel) resistance of the diode should be very large to prevent leakage currents and (ii) that the series resistance should be very small to get a sharp rise in the forward current.

Power conversion efficiency (PCE), (η)

The ratio of power output to power input. In other words, PCE measures the amount of power produced by a solar cell relative to the power available in the incident solar radiation (P_{in}). P_{in} here is the sum of the overall wavelengths and is generally fixed at 100 mW/cm^2 when solar simulators are used. This is the most general way to define efficiency.

$$\eta = \frac{P_{OUT}}{P_{IN}} = \frac{J_{MPP} V_{MPP}}{P_{IN}} = \frac{V_{OC} J_{SC} FF}{P_{IN}} \tag{7}$$

When we consider parasitic resistances such as series resistance (R_S) and shunt resistance (R_{Sh}), the relation between the current density, J, and the voltage, V, therefore is analytically best described by Equation 8.

$$J(V) = J_{SC} - J_0 \left(e^{\frac{q(V + JAR_S)}{kT}} - 1 \right) - \frac{V + JAR_S}{R_{Sh}} \tag{8}$$

Where A represents the photovoltaic cell area.

In the real cell, power is dissipated through the resistance of the contacts and through leakage currents. These effects are equivalent electrically to two parasitic resistances in series (R_S) and in parallel (R_{Sh}) (Figure 2.15c). The series resistance is one of the most important factors influencing the solar cells performance. The series resistance arises from the resistance of the cell material to current flow, particularly through the front surface to the contacts. The parallel or shunt resistance lead currents away from the intended load. Assuming smaller R_S and larger R_{Sh}, the electrical response of the solar cell is expected to consist of three distinctive regimes [49].

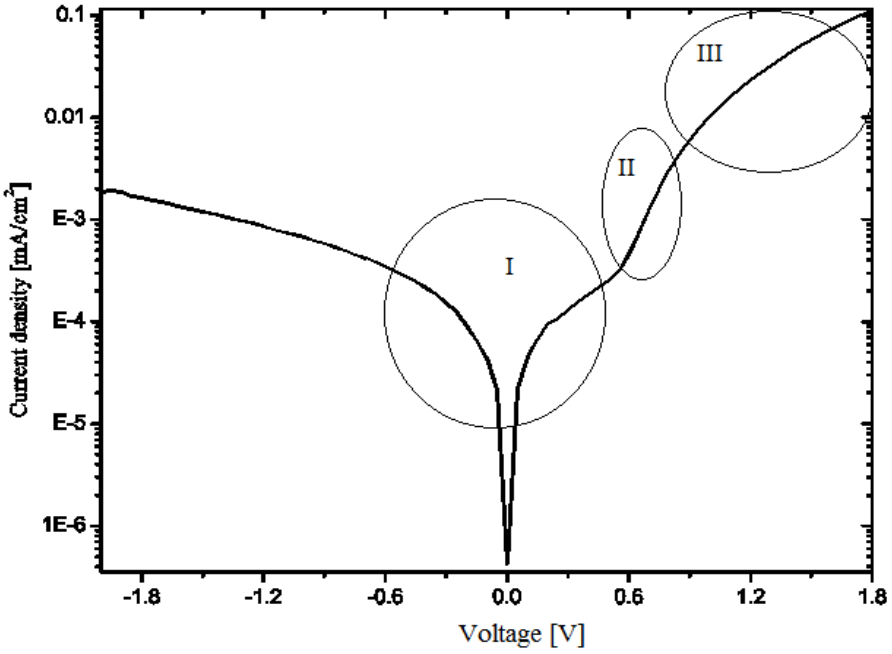

Figure 2.16: Semi logarithmic current density-voltage characteristics of non illuminated bulk heterojunction device.

I. A linear regime at negative voltages and low positive voltages where the current is limited mainly by R_{Sh}.

II. An exponential behavior at intermediate positive voltages where the current is controlled by the diode.

III. A second linear regime at high voltages where the current is limited by the serial resistance R_S.

Series and shunt resistances were derived from the inverse slope of the J-V characteristic curve under dark conditions by using the following equations [50].

$$R_S = \left(\frac{dV}{dI} \right)_{V \to \infty} \tag{9}$$

$$R_{Sh} = \left(\frac{dV}{dI} \right)_{V \to 0} \tag{10}$$

2.4.2 Spectral Response

Incident monochromatic photon-to-current conversion efficiency (IPCE) also called external quantum efficiency is defined as the ratio of the number of collected charge carriers to the number of incident photons at a specific wavelength. It is given by the equation:

$$\text{IPCE} = \frac{1240\, J_{SC}}{\lambda\, P_{in}} \tag{11}$$

Where J_{SC} is short circuit current density ($\mu A/cm^2$), λ the incident photon wavelength (nm) and P_{in} the incident photon intensity (W/m^2).

2.5 Effect of additive on photovoltaic performance of BHJ solar cells

2.5.1 Morphology Control

The nanomorphology of the conducting polymer:fullerene BHJ is a critical factor which affects the polymer solar cell performance [51]. The sizes of the polymer and fullerene phase separated domains in BHJ materials should be 10-20 nm to enable efficient charge transfer and charge separation at the polymer-fullerene interface [52]. In addition, the interpenetrating polymer and fullerene networks must be connected (percolated) through the BHJ so that both holes and electrons can be readily transported to the electrodes. Breaks in the network can form trapping sites for charges, which can be harmful to device performance. Control the formation of a phase separated morphology with crystalline donor acceptor bulk heterojunction solar cells devices were observed by following ways:

(1) By choosing the appropriate solvent with required boiling point for either slow or high evaporation rate [52].

(2) By reducing the drying speed of spin-coated films [53].

(3) By melting of bilayers [54].

(4) By thermal annealing of produced films [14].

(5) By using chemical additives [55].

2.5.2 Processing Additive

The processing additives have been believed to be able to improve the cell performance through altering the bulk heterojunction morphology. In polymer

photovoltaic cell, the charge transport is greatly affected by the morphology of the photoactive layer. The morphological factors, for instance, the interface area between electron donor and acceptor constituents which provides the place for excitons dissociation, the quality of interpenetrating networks including the shape, continuity and orientation with respect to the film plane so as to provide enough highly-efficient pathways for both electrons and holes tobe transported to the correct electrodes, play an important role in determining the device performance [16].

Also “solid” additives could be effective in improving the morphology of BHJ solar cells, as demonstrated for a copolymer based on thienothiophene and pentathiophene units, used as crystallization nucleating agent in P3HT:PCBM active layers [56]. The addition of a few percent by weight of the polymer additive to the P3HT:PCBM solution increased the degree of crystallinity of P3HT and enhanced the performance of the related solar cells. The exciton binding energy in organic semiconductors is generally large ($\approx$0.4 eV) the built in electric fields (on the order of 10^6-10^7 V/m) are usually not high enough to dissociate the excitons directly [38]. The thermodynamic requirement for an exciton to dissociate at an interface is that the band offset must be greater than the exciton binding energy [57]. The kinetic factors controlling the probability of exciton dissociation at interfaces (or trap sites) are not well understood. It is not known, for example, why organic/organic interfaces are often much more efficient for exciton dissociation than organic/inorganic interfaces [58]. Moreover, there is a tradeoff between rapid exciton motion and efficient quenching. The interfacial electron transfer (quenching) rate must compete with the residence time of the exciton at the interface; thus, rapid exciton transport, while otherwise beneficial, can require ultrafast quenching at the interface for efficient carrier production [58].

There is another factor that affects the interfacial residence time: the exciton energy at the interface can be greater than or less than that in the bulk depending on the lower or higher, respectively, polarizability of the contacting phases [59]. If the polarizability is higher, it tends to trap the exciton near the interface and thus promote dissociation; if the polarizability is lower, the exciton will tend to be reflected from the interface back into the bulk. Interface adhesion ("wetting"), or its absence, can play a role similar to the polarizability. There is also another factor that affects exciton dissociation at an interface the increased dielectric constant of the matrix increases the screening of photogenerated electrons and holes and, thus, facilitates the charge separation [60]. Through the proper choice of additive the exciton dissociation at the donor acceptor interface could be advantageously tuned. In this thesis propylthiouracil, a small molecule solid, has been used as the additive in the P3HT and PCBM blend system.

3. Objectives

3.1 General Objectives

- The general objective of this research is to study the effect of chemical additive on photovoltaic characteristics of bulk heterojunction solar cells based on poly(3-hexylthiophene) (P3HT) and [6,6]-phenyl C_{61} butyric acid methyl ester (PCBM).

3.2 Specific Objectives

- To construct organic solar cells from poly(3-hexylthiophene) (P3HT) and [6, 6]-phenyl C_{61} butyric acid methyl ester (PCBM) with different concentration of propylthiouracil.
- To characterize the solar cells using various standard characterization techniques such as I-V, IPCE, etc.
- To show the consistency of IPCE with absorption spectrum of the blend, (P3HT:PCBM with different concentration of propylthiouracil).
- To identify which parameters are affected by the addition of propylthiouracil in P3HT:PCBM BHJ solar cells.

4. Materials and methods

4.1. Materials

The materials that were used for the construction of bulk heterojunction solar cells are a transparent conductive bottom electrode, indium doped tin oxide (ITO) coated on flat glass substrates, P3HT, and PCBM, used as photoactive materials, a poly(3, 4-ethylene dioxythiophene):poly(styrenesulfonate) (PEDOT:PSS) used to facilitate charge injection and extraction, improves the workfunction of the anode (usually, ITO/PEDOT:PSS system is regarded as the "anode"), providing a better matching with the HOMO of donor energy level. It also acts as an electron-blocking layer and smooths the roughness of ITO surface, thus minimizing the occurrence of short-circuits [61], propylthiouracil were used as additive. The chemical structures of the substances used in this work are depicted in Figure 4.1.

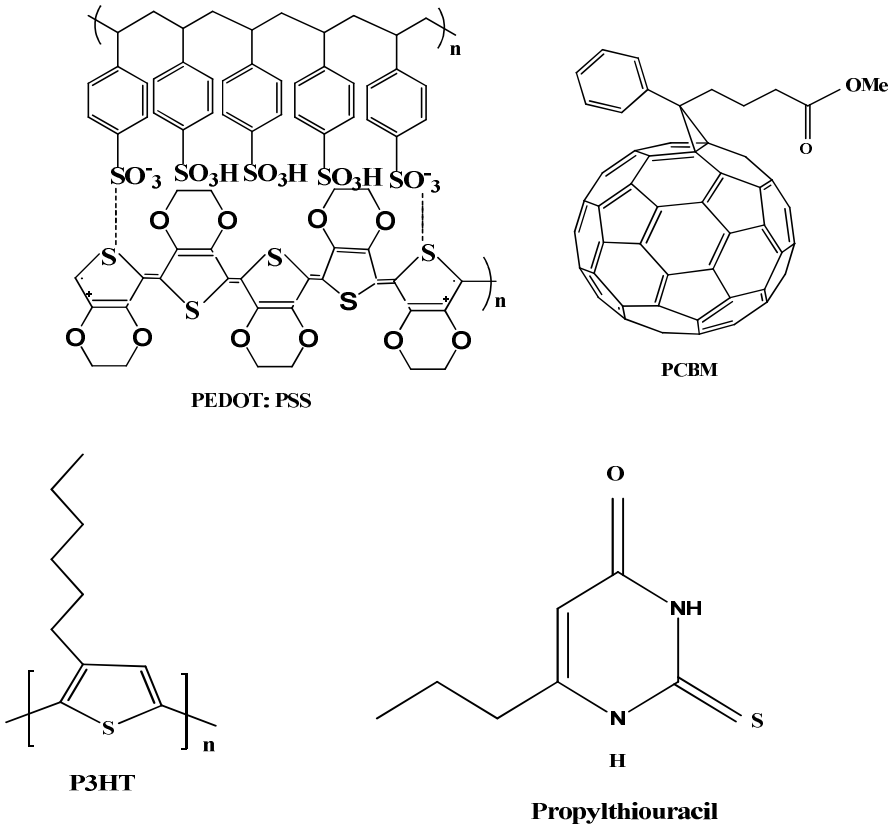

Figure 4.1: Chemical structure of substances used in this work.

4.2. Experimental methods

Conducting polymer based organic solar cell generally consists of a transparent conductive bottom electrode, indium doped tin oxide (ITO) coated on flat glass substrates. A poly(3, 4-ethylenedioxythiophene):poly(styrenesulfonate) (PEDOT:PSS) layer is spin coated on top of ITO layer to facilitate charge injection and extraction. The light absorbing organic layer, poly(3-hexyltheiophene) (P3HT) and [6, 6]-phenyl C_{61} butyric acid methyl ester (PCBM), is deposited by spin-coating technique on top of PEDOT:PSS. The upper electrode can be generally formed by vacuum deposition of low work function metal aluminum (Al), onto photoactive layer. Aluminum is a common metal electrode used in photovoltaics to collect the electrons.

4.3 Fabrication of solar cells

The fabrications of solar cells were done in 5 steps. (1) Cleaning of substrate, (2) Preparation of polymer solution (3) Spin coating of PEDOT:PSS, (4) Spin coating of P3HT:PCBM with different concentration of propylthiouracil and (5) Vacuum deposition of Al.

4.3.1 Cleaning of substrate

ITO coated glass substrates were cleaned sequentially by using acetone, isopropanol, and ethanol for 20 min in an ultrasonic bath.

4.3.2 Preparation of solution

1 mg and 1.5 mg propylthiouracil were dissolved separately in 10 ml chlorobenzene and stirred overnight. The photoactive solutions were prepared by dissolving P3HT (10 mg) and PCBM (10 mg) in 1 ml chlorobenzene (without additive), and with the addition of 0.75% (w/w), 1% (w/w), and 1.5% (w/w) propylthiouracil to the P3HT (10 mg) and PCBM (10 mg) mixture. Then the mixtures were stirred overnight.

4.3.3 Spin coating

The PEDOT:PSS was spin coated on top of the cleaned ITO coated glass substrate at spin rate of 4000 rpm for 46 s. This was followed by annealing the film at 150 ^{0}C for 10 minutes, leaving a dried thin film. The PEDOT:PSS layer improves the quality of the ITO electrode. The surface roughness of the ITO is minimized and the electric contact to the active layer is improved. Then, P3HT:PCBM solution with different concentration of propylthiouracil additive was spin coated on top of PEDOT:PSS at 800 rpm for 41 s yielding thin film spread over the whole plate as active layer. Spin coating was done by using SCS 6800 spin coater series. For electrical contact some part of the polymer film is removed from the etched part using toluene. Finally the low work function metal aluminum (Al) is thermally deposited partly on the active area film and partly on the clean glass using a mask. The deposition was done using Edward Auto 306 vacuum evaporator, at pressure in the chamber of the evaporator is reduced about 4×10^{-6} mbar. As a source, tungsten boat was used. After aluminum is evaporated, the device was taken out of the chamber for characterization. The final sandwich type devices of bulk heterojunction solar cell of ITO/PEDOT:PSS/P3HT: PCBM/Al is depicted in Figure 4.2.

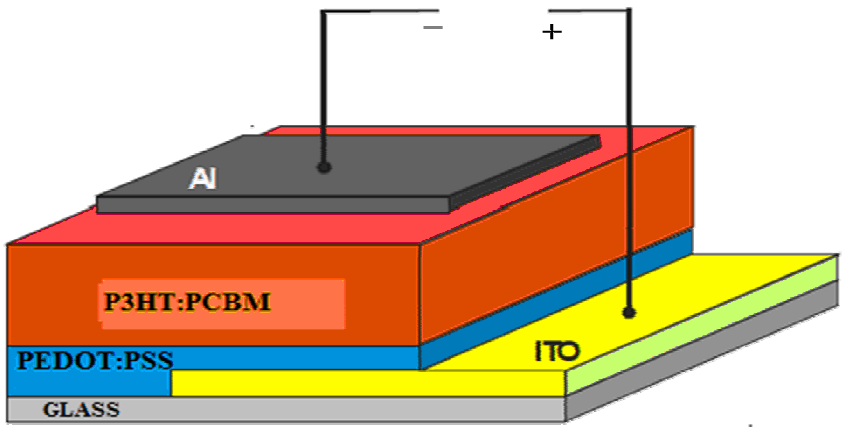

Figure 4.2: Basic device structure of bulk heterojunction solar cell used in this study.

4.3.4. Device characterization

The current-voltage (I-V) characteristic in the dark, as well as under illumination was measured by using HP 4140B pA meter/DC voltage source, together with HP 16055A-test fixture. The measurement was taken by continuously sweeping the voltage applied from -2 V to 2 V at 10 mV steps with hold time and step delay time of 1 s. The I-V measurement under illumination was carried out by mounting inside the sample holder under a standard sun illumination, using a solar simulator model SS-50AA the intensity of light incident on the cell was about 80 $mWcm^{-2}$. IPCE characterizations of the solar cell were performed using a computer controlled CHI630A instrument. A 150 W Xenon lamp regulated by an Oriel power supply (Model 68830) was used to illuminate the solar cells. A grating monochromator (Model 77250) placed into the light path was used to select a wavelength manually between 300 nm and 800 nm at an interval of 10 nm. The measured photocurrent spectra were corrected for the spectral response of the lamp and the monochromator by normalization to the response of a calibrated silicon photodiode (Hamamatsu, Model S-1336-8BK) whose sensitivity spectrum was known. No correction was made for the reflection from the surface of the sample. The white light intensity was measured in the position of the sample cell with Gigahertz-Optik (model X1-1) Optometer. The intensity of the incident light was 100 mW/cm^2. Optical absorption measurements were carried out using UV-Vis Spectrophotometer (Spectronic GENESIS, USA)

5. Results and Discussion

5.1 Absorption Spectra Measurement

It is well established that conjugated polymer solid-state UV-visible absorption spectra are strongly influenced by the molecular packing and can be used to investigate the degree of P3HT molecular structural ordering. We, therefore, investigated the absorption spectra of P3HT:PCBM with different concentration of propylthiouracil blends spin coated onto glass substrates from chlorobenzene solutions. The resulting absorption spectra are displayed in Figure 5.1. For each blend, the absorption spectrum has been normalized to the PCBM peak (around 330 nm). The results show that the absorption edge is red shifted and that the vibrational structure of the P3HT absorption band is more pronounced when propylthiouracil is added to the blend. This implies better stacking/ordering of P3HT because a closer π stacking of P3HT chains can lead to a lower band-like energy [62]. Closer π-stacking of P3HT chains can contribute to an enhancement in J_{SC} due to a lower resistance to the hopping of carriers between P3HT backbones. From the chemical structure of propylthiouracil and PCBM the common carbonyl functional group leads to higher miscibility of propylthiouracil additive in PCBM than P3HT. The addition of additives with a selective miscibility in one of the components of BHJ films is known to improve the morphology of the photoactive layer for charge separation and transport, which ultimately improves device characteristics [63]. The relatively better miscibility of propylthiouracil additive with PCBM molecules in the bulk resulted in a phase separation between P3HT and PCBM, which can contribute to the formation of larger PCBM domains. Thus, the existence of propylthiouracil is considered to lead to the formation of slightly larger PCBM domains, while most PCBM in the device

without additive is molecularly dispersed within a P3HT matrix [64]. Hence, the selectively dispersed propylthiouracil additive facilitate the formation of bicontinuous phase separation between P3HT and PCBM to provide better bicontinuous pathways for the holes and electrons. The higher stacking/aggregation also plays an important role in increasing charge transport in the active layer, contributing to the high current density of device.

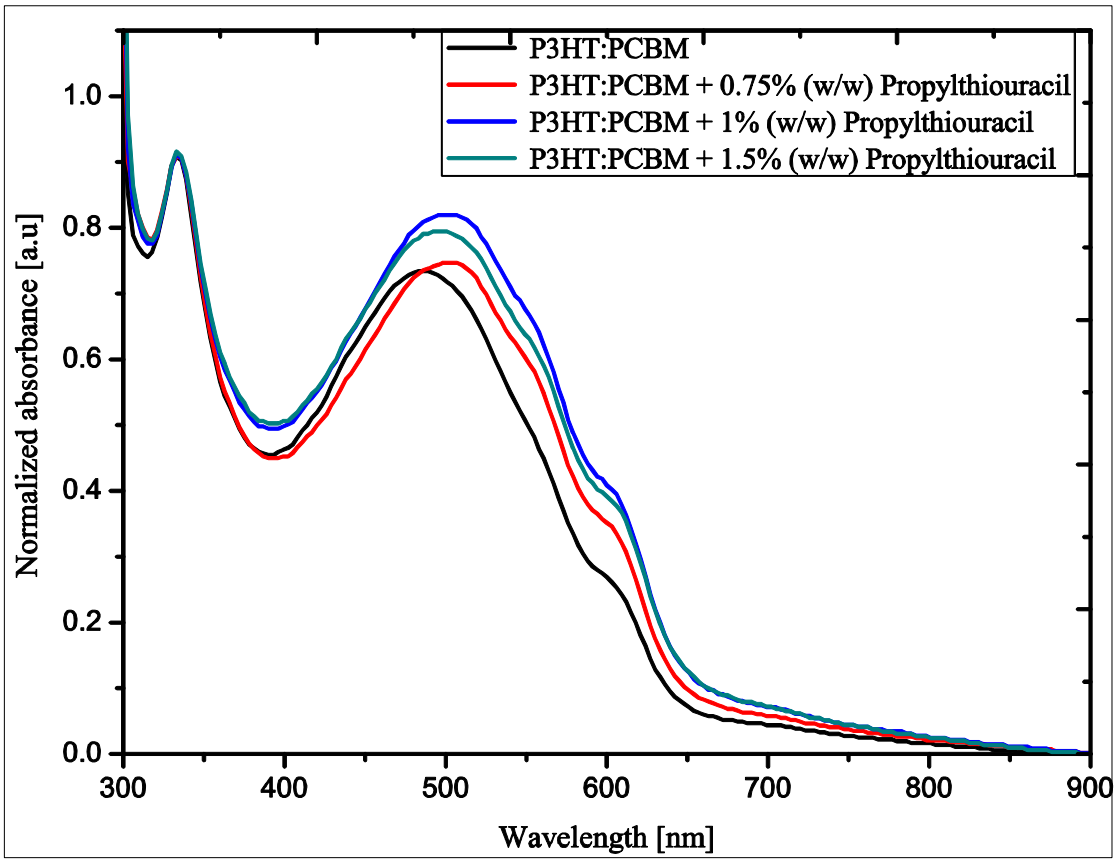

Figure 5.1: Normalized absorbance of thin films of P3HT:PCBM with different concentration of propylthiouracil.

5.2 Current Density-Voltage (J-V) Characteristics

Dark current density-voltage (J-V) curves recorded for all four different solar cells made at different concentration of propylthiouracil are shown in Figure 5.2. The dark (J-V) characteristic of a P3HT:PCBM with different concentration of propylthiouracil device has three distinct regimes: at low voltage the measured current is dominated by local leakage currents due to weak spots in the film, giving rise to Ohmic behavior, which is symmetric for reverse bias. An exponential behavior at intermediate positive voltages where the current is controlled by the diode and at high voltages where the current is limited by the serial resistance R_S.

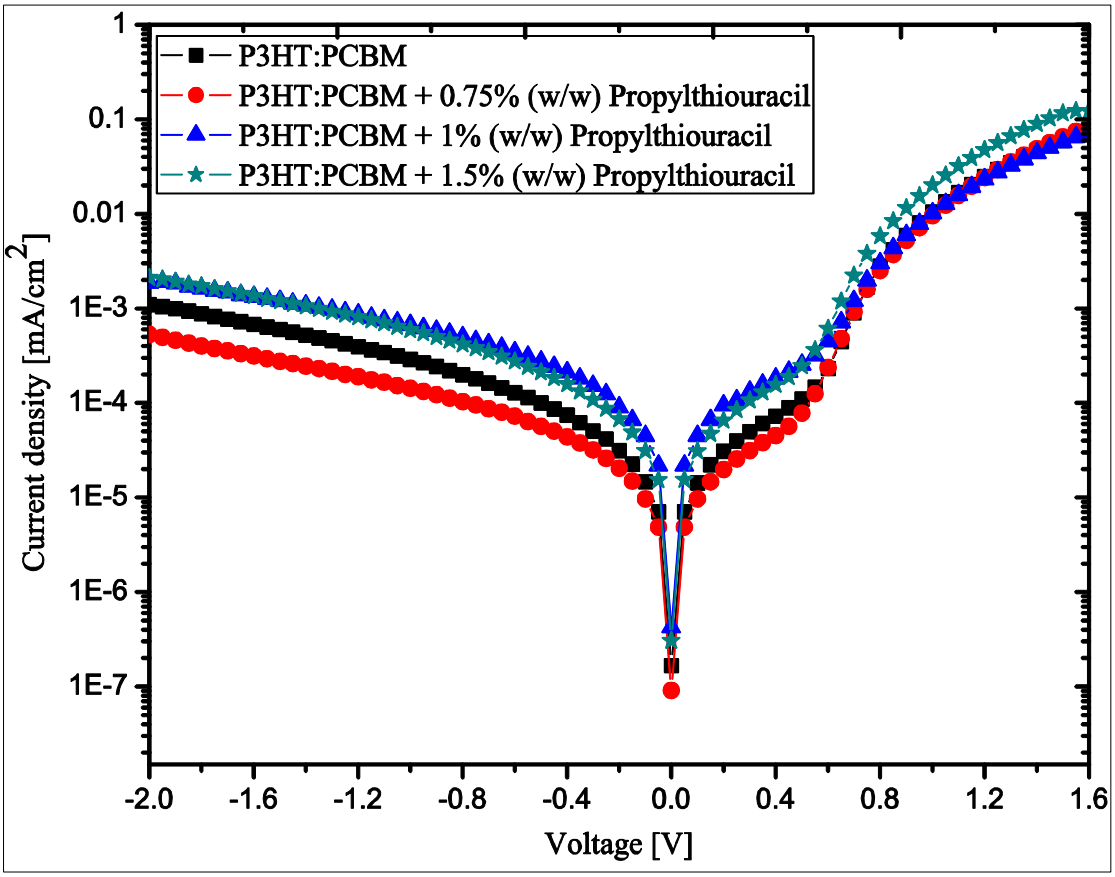

Figure 5.2: Semilogarithmic current density-voltage characteristics of bulk heterojunction device of structure ITO/PEDOT:PSS/P3HT:PCBM with different concentration of propylthiouracil/Al.

Figure 5.3 and 5.4**.** shows the current density (J)-voltage (V) curves of P3HT:PCBM BHJ solar cells constructed using different concentration of propylthiouracil additives. For comparisons the device without additive also included, the data obtained from the graph are summarized in Table 1.

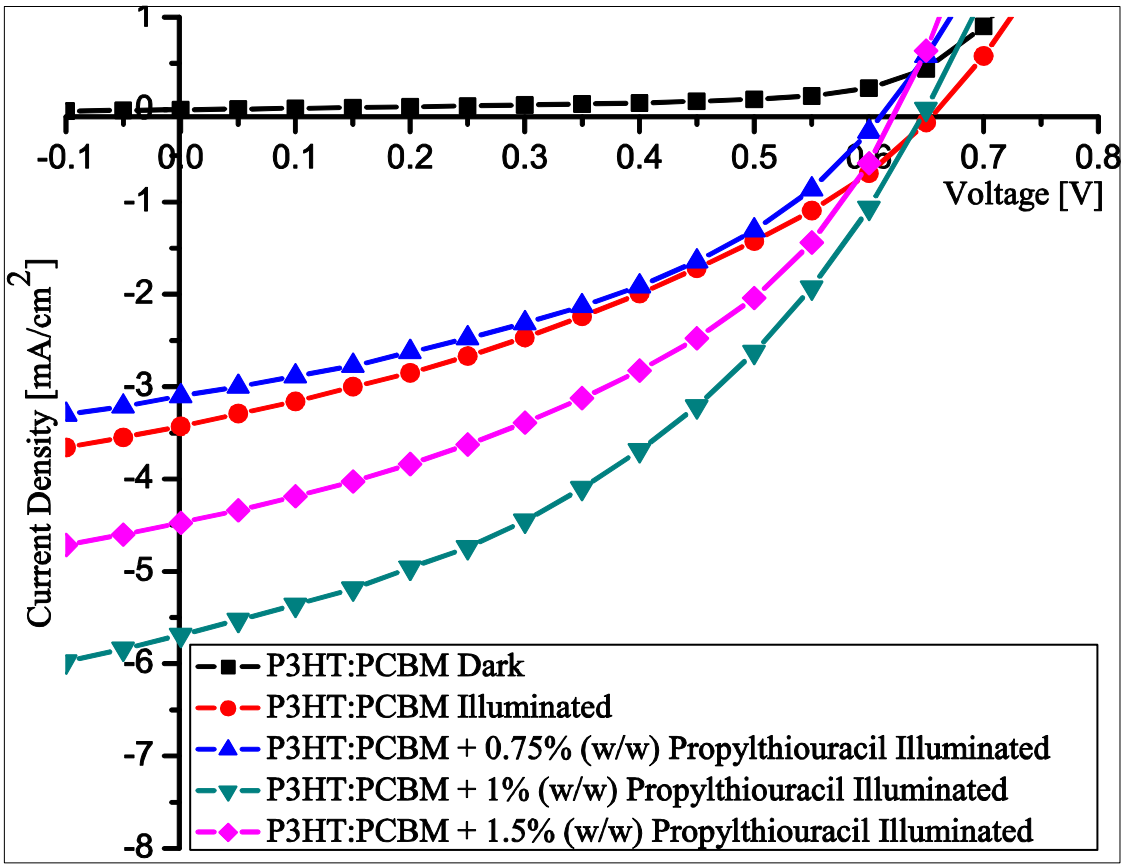

Figure 5.3: The J-V characteristics of ITO/PEDOT:PSS/P3HT:PCBM/Al, based BHJ solar cell with different concentration of propylthiouracil additive in the dark and under white light illumination with incident light intensity of 80 mW/cm^2.

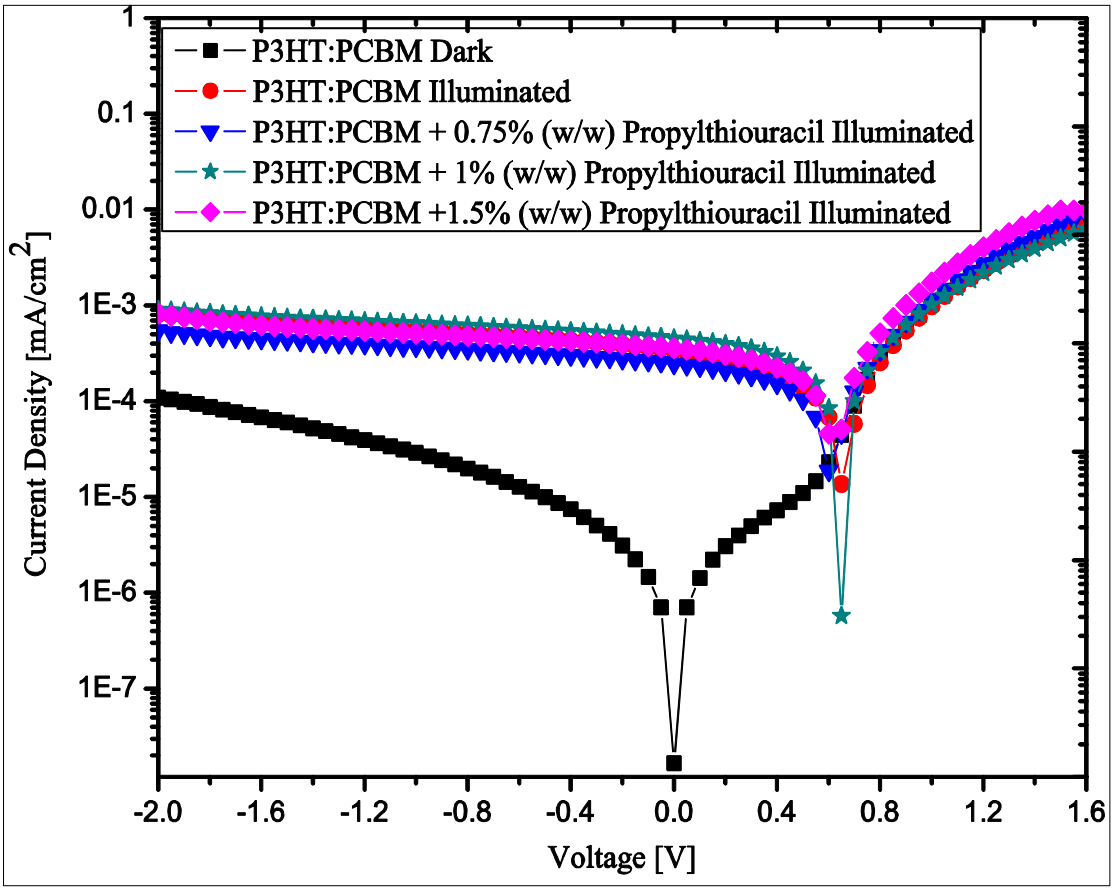

Figure 5.4: Semilogarithmic J-V characteristics of ITO/PEDOT:PSS/P3HT:PCBM /Al, based BHJ solar cell with different concentration of propylthiouracil additive in the dark and under white light illumination with incident light intensity of 80 mw/cm^2.

Table 1: The typical photovoltaic performance parameters of P3HT:PCBM with different concentration of propylthiouracil (PTU) additive at illumination intensity of 80 mw/cm^2.

Active Layer	R_S (Ω cm^2)	V_{OC} (V)	J_{SC} (mA/cm^2)	FF (%)	Efficiency (%)
P3HT:PCBM	15	0.660	3.43	35	1.0
P3HT:PCBM + 0.75% (w/w) Propylthiouracil	20	0.610	3.20	37	0.9
P3HT:PCBM + 1% (w/w) Propylthiouracil	8	0.648	5.69	40	1.8
P3HT:PCBM + 1.5% (w/w) Propylthiouracil	14	0.623	4.47	41	1.4

The device without additive shows V_{OC} of 0.66 V, J_{SC} of 3.43 mA/cm^2, FF of 35%, and power conversion efficiency (PCE) of 1%. After addition of 0.75% (w/w) propylthiouracil, V_{OC} decreased from 0.66 V to 0.61 V, J_{SC} decreased from 3.43 mA/cm^2 to 3.20 mA/cm^2, which in turn reduces the PCE from 1% to 0.9%. The reason might be due to the insufficient concentration of propylthiouracil that do not lead to phase separation rather increases the serial resistance from 15 Ω cm^2 to 20 Ω cm^2. But as concentration increases to 1% (w/w), the current increases as a result of good phase separation as confirmed from the decrease in serial resistance to 8 Ω cm^2. When we further increase the concentration of propylthiouracil to 1.5% (w/w) still J_{SC} increases but as compared to 1% (w/w), it is decreasing due to the increase in serial resistance from 8 Ω cm^2 to 14 Ω cm^2. Thus, the most effective propylthiouracil content is 1% (w/w), where the BHJ solar cell device exhibits the best performance, this shows that the concentration of propylthiouracil at around 1% (w/w) is the optimum that leads to decrease in serial resistance and increase in J_{SC}. Another possible reason might be the increased dielectric constant of the matrix, due to polar nature of propylthiouracil that increases the screening of photo-generated electrons and holes and, thus, facilitates the charge separation. The low V_{OC} in additive

processed devices is attributed to the upward shift in the HOMO level of P3HT as a result of its aggregation [53].

The current density-voltage characteristics of ITO/PEDOT:PSS/P3HT:PCBM/Al based bulk heterojunction solar cell, without additive and with 1% (w/w) propylthiouracil, are shown in Figure 5.5 and 5.6, respectively.

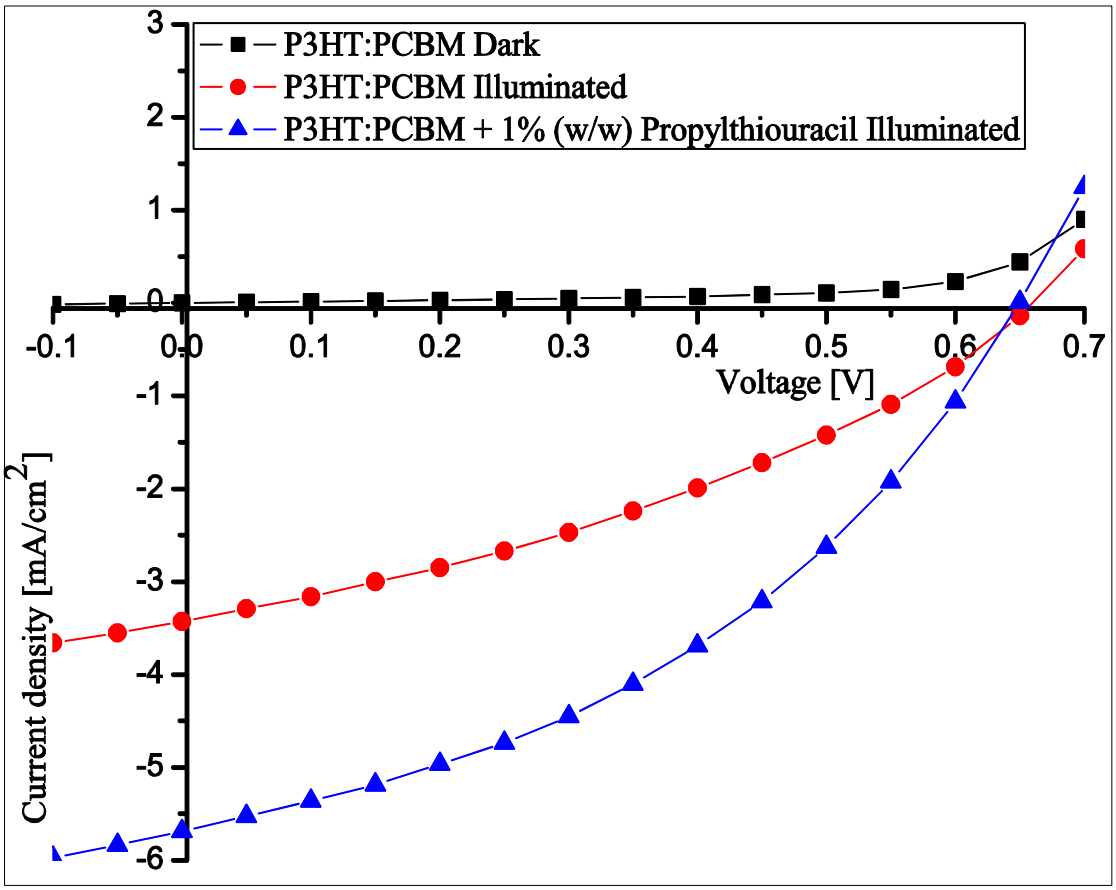

Figure 5.5: Current density-voltage characteristics of bulk heterojunction device of structure ITO/PEDOT:PSS/P3HT:PCBM/Al, in the dark and under white light illumination with incident light intensity of 80 mw/cm^2.

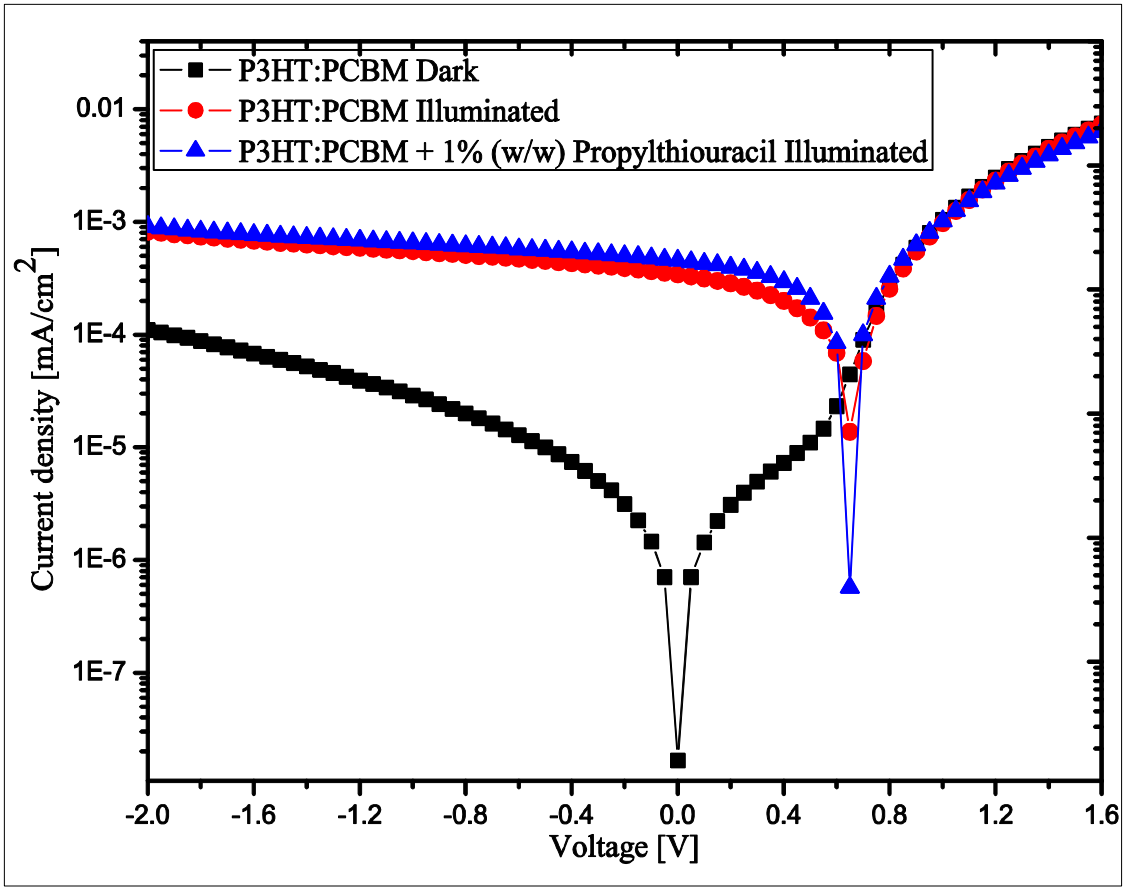

Figure 5.6: Semilogarithmic current density-voltage Characteristics of bulk heterojunction device of structure ITO/PEDOT:PSS/P3HT:PCBM/Al, in the dark and under white light illumination with incident light intensity of 80 mW/cm^2.

The photovoltaic performance parameters of device before addition of propylthiouracil additive shows V_{OC} = 0.66 V, J_{SC} = 3.43 mA/cm^2, and FF= 35%. The power conversion efficiency (η) was calculated using equation (6) is therefore 1%. With addition of 1% (w/w) propylthiouracil additive J_{SC} increased from 3.43 mA/cm^2 to 5.69 mA/cm^2 and the FF from 35% to 40%, which lead to an enhancement of PCE from 1% to 1.8%.

5.3 Spectral Response

The dependence of the photovoltaic performance on the propylthiouracil content was further confirmed by the incident monochromatic photon to current conversion efficiency (IPCE) measurement of the devices, as shown in Figure 5.7. The IPCE curves of the devices with different propylthiouracil contents show maximum IPCE around 62% in the wavelength range of 480-510 nm, corresponding to the absorption maxima of the blend. With increasing the propylthiouracil content from 0% (w/w) to 0.75% (w/w) to 1% (w/w) then to 1.5% (w/w), the IPCE maximum decreased from 55% to 44%, and then increased to 62%, finally decreased to 59%. The IPCE profile varying with the propylthiouracil content is consistent with that for J_{SC} and PCE.

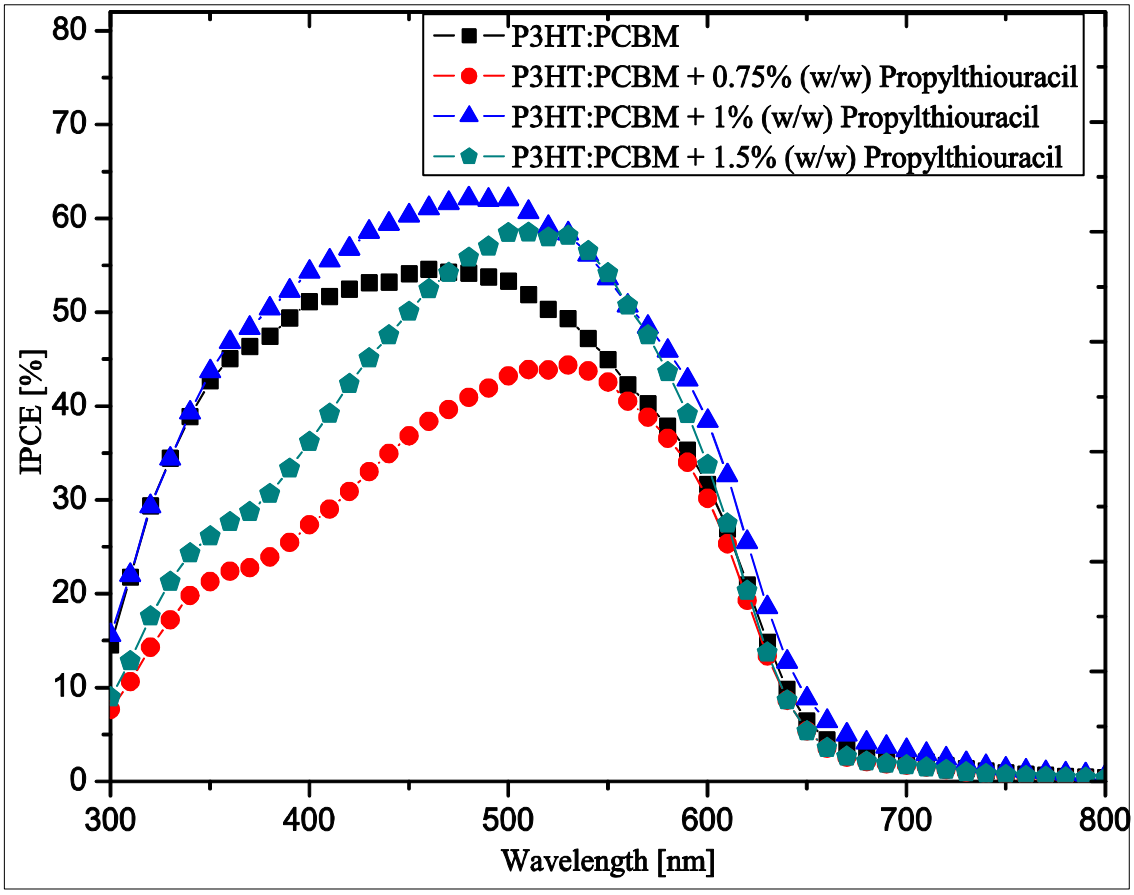

Figure 5.7: IPCE spectra of bulk heterojunction device of structure ITO/PEDOT: PSS/P3HT:PCBM/Al, with different concentration of propylthiouracil additives.

5.4 Comparison between Optical Absorption and Spectral Response

Comparing the spectral response of the solar cells and the optical absorption spectra of the devices, information on the charge-generation mechanism can be obtained [65]. Figure 5.8 shows comparison between the IPCE and absorption spectra of bulk heterojunction solar cells that are investigated in this study.

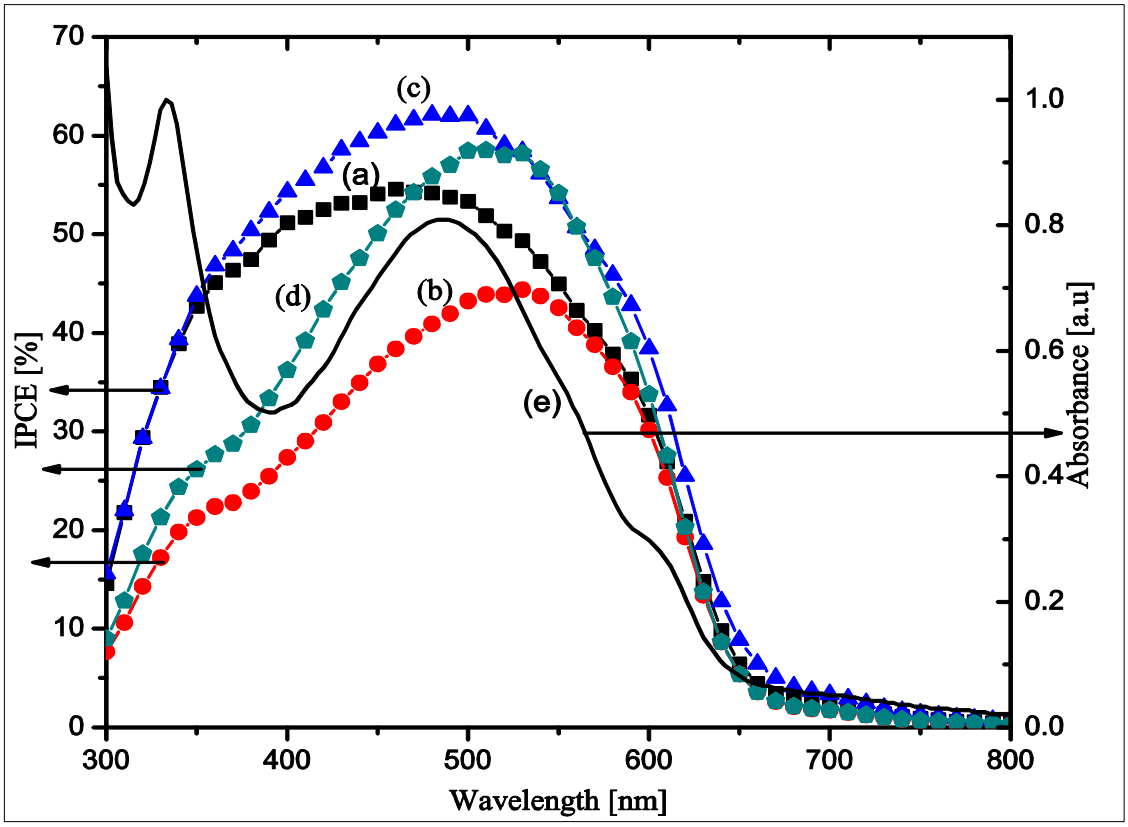

Figure 5.8: IPCE spectra of bulk heterojunction device of structure ITO/PEDOT: PSS/P3HT: PCBM/Al. (a) without additive (b) with 0.75% (w/w) propylthiouracil (c) with 1% (w/w) propylthiouracil (d) with 1.5% (w/w) propylthiouracil (e) absorption spectra of P3HT:PCBM.

Increased J_{SC} is mainly related to more exciton and charge generations and more effective charge transport. To probe the role of propylthiouracil in this system, effect of propylthiouracil on absorption spectra of P3HT:PCBM films was examined to have an insight into the generations of excitons and charge carriers. The film with 1% (w/w) propylthiouracil content exhibits stronger absorption than that without propylthiouracil, while when 0.75% (w/w), and, 1.5% (w/w), propylthiouracil was added, a drop in absorbance was observed. The stronger absorption partially contributed to higher J_{SC} and IPCE of the device processed with 1% (w/w) propylthiouracil compared to the others. It can be seen clearly that optical absorption matches the IPCE spectra.

6. Conclusion

In this study organic bulk heterojunction solar energy conversion device based on blend of poly(3 hexylthiophene) (P3HT) and [6, 6]-phenyl C_{61} butyric acid methyl ester (PCBM) with different concentration of propylthiouracil additive were fabricated and studied. Short circuit current density (J_{SC}), open circuit voltage (V_{OC}), fill factor (FF), and power conversion efficiency of device without additive is found to be 3.43 mA/cm^2, 0.66 V, 35%, and 1%, respectively. This device showed an IPCE of 55% at 460 nm. In order to see the effect of propylthiouracil additive on the photovoltaic performance of the device we performed optimization on the weight ratio of the additives according to the photovoltaic performance of the devices and found that 1% (w/w) is the best. The optical absorption results clearly indicate that the absorption edge is red shifted and that the vibrational structure of the P3HT absorption band is more pronounced when propylthiouracil is added to the blend. This implies better stacking/ordering of P3HT because a closer π stacking of P3HT chains can lead to a lower band-like energy [62]. Closer π-stacking of P3HT chains can contribute to an enhancement in J_{SC} due to a lower resistance to the hopping of carriers between P3HT backbones. The short circuit current density (J_{SC}), open circuit voltage (V_{OC}), fill factor (FF), and power conversion efficiency of 1% (w/w) propylthiouracil additive processed device is found to be 5.69 mA/cm^2, 0.648 V, 40%, and 1.8% , respectively. The device showed an IPCE of 62% at 480 nm. Our results also show that addition of 1% (w/w) propylthiouracil additive to P3HT:PCBM BHJ solar cell improve efficiency of the device from 1 to 1.8%.

References

[1] T.M. Razykov, C.S. Ferekides, D. Morel, E. Stefanakos, H.S. Ullal, H.M. Upadhyaya, *Solar Energy*. 85 (2011) 1580.

[2] Key World Energy Statistics, *International Energy Agency*, Paris, (2006) p46.

[3] Q. Y. Meng and R. W. Bentley, *Energy,* 33 (2008) 1179.

[4] J. Goldemberg, T. B. Johansson, World Energy Assessment Overview**,** New York, 2004.

[5] J. L. Stone, Photovoltics: Unlimited electrical energy from the sun, *physics today* (1993) P23.

[6] J. Zhao, A. Wang, M.A. Green, F. Ferrazza, *Appl. Phys. Lett.* 73 (1998) 1991.

[7] L. Tsakalakos, *Materials Science and Engineering.* 62 (2008) 175.

[8] S. Gunes, H. Neugebauer and N.S. Sariciftci, *Chem. Rev*. 107 (2007**)** 1324.

[9] N. S. Sariciftci, L. Smilowitz, A. J. Heeger, F.Wudl, *Science,* 258 (1992*)* 1474.

[10] H. Hoppe, N.S. Sariciftci, D. Meissner, *Mol. Cryst. Liq. Cryst*. 385 (2002) 113.

[11] M. Schwoerer, and H. Wolf, Organic molecular solids, Wiley Online Library, (2007).

[12] S. Forrest, The limits to organic photovoltaic cell efficiency, MRS bulletin. 30 (2005) 28.

[13] C. Brabec, N. S. Sariciftci, J. Hummelen, *Adv. Funct. Mater*. 11 (2001) 15.

[14] F. Padinger, R. S. Rittberger, N. S. Sariciftci, *Adv. Funct. Mater*. 13 (2003) 1.

[15] A. Pivrikas. *Solar Energy*. 85 (2011) 1226.

[16] J. K. Lee, W. Ma, C. J. Brabec, J. Yuen, J. S. Moon, J. Y. Kim, K. Lee, G. C. Bazan, A. J. Heeger, *J. Am. Soc. Chem.* 130 (2008) 3619.

[17] S. Roth, H. Bleier, W. Pukacki**,** *Chem. Soc*. 88 (1989) 223.

[18] Handbook of Conducting Polymers (Eds.: T. A. Skotheim, R. L. Elsenbaumer, J. R. Reynolds), 2nd ed., Marcel Dekker, New York, 1998.

[19] C. K. Chiang, C. R. Fincher, Jr., Y. W. Park, A. J. Heeger, H. Shirakawa, E. J. Louis, S. C. Gau, A. G. MacDiarmid, *Phys. Rev. Lett*. 39 (1977) 1098.

[20] A. J. Heeger, *Rev. Mod. Phys*. 73 (2001) 681.

[21] W. R. Salaneck, R. H. Friend, J. L. Brédas, *Phys. Rep. Rev. Sec. Phys. Lett*., 319 (1999) 231.

[22] A. J. Heeger, S. Kivelson, J. R. Schrieffer, and W.P. Su, *Rev. Mod. Phys*. 60 (1988) 781.

[23] J. Rasmusson, S. Stafström, M. Lögdlund, W.R. Salaneck, U. Karlsson, D.B.Swanson, A.G. MacDiarmid, G.A. Arbuckle, *Synth. Met*. 41 (1991) 1865.

[24] A. G. MacDiarmid, Angew. *Chem. Int. Ed*. 40 (2001) 2581.

[25] J. L. Bredas, R. R. Chance, R. Silbey, *Mol. Crys. Liq. Crys*. 77 (1981) 319.

[26] W. R. Salaneck, H. R. Thomas, C. B. Duke, E. W. Plummer, A. J. Heeger, A. G. Mac Diarmid, *J. Chem. Phys*. 71 (1979) 2044.

[27] J. Tanaka, C. Tanaka, T. Miyamae, K. Kamiya, M. Shimizu, M. Oku, K. Seki, J.Tsukamoto, S. Hasegawa, H. Inokuchi, *Synth. Met.* 55 (1993) 121.

[28] G. Hadziioannu, P. F. Van Hutten; “Semiconducting Polymers, Chemistry Physics and Engineering”; Wiley, Weinheim, 2000.

[29] S. Kuroda, H. *Shirakawa*, *Synth. Met*. 17 (1987) 423.

[30] Y. Onodera, *Phys. Rev. B.* 30 (1984) 301.

[31] P. Chandrasekhar, Conducting Polymers, Fundamentals and Applications: A Practical Approach, Kluwer Academic Publishers, New York, 1999.

[32] A. O. Patil, A. J. Heeger, F. Wudl, *Chem. Rev*. 88 (1988) 183.

[33] M. Mastragostino, C. Arbizzani, A. Bongini, G. Barbarella, M. Zambianchi,

Electrochim. Acta. 38 (1993) 135.

[34] J. Przyluski, Solid State Phenomena, Vol 13 and 14, Scien-Tech Publication Ltd, Liechtenstein, 1991, pp120-175.

[35] N.T. Kemp, G.U. Flanagan, A.B. Kaiser, H.J. Trodahl, B. Chapman, A.C. Partridge and R.G. Buckley. *Synthetic Metals.* 101 (1999) 434.

[36] S. Kivlson, *Phys. Rev. B.* 25 (1982) 3798.

[37] H. Hoppe, *J. Mater. Res.* 19 (2004) 1924.

[38] Tom Aernouts, PhD dissertation, 2006, ISBN: 90-8649-048-4.

[39] R. N. Marks, J.J.M. Halls, D.D.C. Bradley, R.H. Friend and A.B. Holmes, *J. Phys.:Condens. Matter.* 6 (1994) 1379.

[40] C. W. Tang, *Appl. Phys. Lett*. 48 (1986) 183.

[41] N. S. Sacriciftci, D. Braun, C. Zhang, V.I. Srdanov, A.J. Heeger, G. Stucky, F. Wudl, *Appl. Phys. Lett.* 62 (1993) 585.

[42] Z. R. Hong, B. Maennig, R. Lessmann, M. Pfeiffer, K. Leo, P. Simon, *Appl. Phys. Lett.* 90 (2007) 203505.

[43] R. Koeppe, N. S. Sariciftci, P. A. Troshin, R. N. Lyubovskaya, *Appl. Phys. Lett*. 87 (2005) 244102.

[44] G. Yu and A. J. Heeger, *J. Appl. Phys.* 78 (1995) 4510.

[45] Gang Li *et al.*, *Nature Materials*. 4 (2005) 864.

[46] H. Spanggaard, F. C Krebs, *Solar Energy Materials & Solar Cells.* 83 (2004) 125.

[47] Zheng Tang, Master Thesis, 2010, ISBN, ISRN: LITH-IFM-A-EX--10/2009—SE.

[48] M. A. Green, K. Emery, Y. Hishikawa , W. Warta, *Prog. Photovolt: Res. Appl.* 19 (2011) 84.

[49] V. D. Mihailetchi, P. W. M. Blom, J. C. Hummelen and M. T. Rispens, *J. Appl. Phys*. 94 (2003) 6849.

[50] F. Shirland, *Adv. Energy Conversion.* 6 (1966) 201.

[51] H. Hoppe, M. Niggemann, C. Winder, J. Kraut, R. Hiesgen, A. Hinsch, D. Meissner, N. S. Sariciftci, *Adv. Funct. Mater*. 14 (2004) 1005.

[52] S. E. Shaheen, C. J. Brabec, N. S. Sariciftci, *Appl. Phys. Lett*. 78 (2001) 841.

[53] G. Li, V. Shrotriya, J. Huang, Y. Yao, T. Moriarty, K. Emery, Y. Yang, *Nat. Mater*. 4 (2005) 864.

[54] K. Kim, J. Liu, D.L. Carroll, *Appl. Phys. Lett*. 88 (2006) 181911.

[55] J. Peet, J. Y. Kim, N. E. Coates, W. L. Ma, D. Moses, A. J. Heeger, G. C. Bazan, *Nat. Mater.* 6 (2007) 497.

[56] R. Bechara, N. Leclerc, P. Le´veˆque, F. Richard, T. Heiser, G. Hadziioannou, *Appl. Phys. Lett*. 93 (2008) 013306.

[57] B. A. Gregg; *J. Phys. Chem.*107 (2003) 4688.

[58] B. A. Gregg, J. Sprague, M. Peterson, *J. Phys. Chem.* 101 (1997) 5362.

[59] A. Zakhidov, K. Yoshino, *Synth. Met*. 64 (1994) 155.

[60] B. Yang, J. Cox, Y. Yuan, F. Guo, and J. Huang, *Appl. Phys. Lett*. 99 (2011) 133302.

[61] R. Po, M. Maggini, and N. Camaioni, *J. Phys. Chem. C.* 114 (2010) 695.

[62] P. J. Brown, D. S. Thomas, A. Ko¨hler, J. S. Wilson, J.S. Kim, C.M. Ramsdale, H. Sirringhaus, R. H. Friend, *Phys. Rev. B.* 67 (2003) 064203.

[63] Y. Yao, J. Hou, Z. Xu, G. Li, Y. Yang, *Adv. Funct. Mater*. 18 (2008) 1783.

[64] D. Chirvase, J. Parisi, J. C. Hummelen, V. Dyakonov, *Nanotechnology*. 15 (2004) 1317.

[65] J. Rotalsky and D. Meissner, *Sol. Energy. Mater. Sol. Cells.* 63 (2000) 37.